Mathematical Modelling of Metastatic Processes on a Network

Khimeer Singh

Supervised by Professor Byron Jacobs

UNIVERSITY OF THE
WITWATERSRAND,
JOHANNESBURG

School of Computational and Applied Mathematics

Declaration

I, **Khimeer Singh**, declare no portion of this work referred to in this project entitled *Mathematical Modelling of Metastatic Processes on a Network* has been submitted in support of an application for another degree or qualification of this or any other university or other institution of learning. All information from other sources has been duly referenced and acknowledged.

Khimeer Singh — Khimeer Singh

09/06/2022 — Date

Acknowledgements

First and foremost, I would like to thank my supervisor, Prof. Byron Jacobs. Not only for his valued council - of which I am hugely appreciative - but also for his willingness to explore the stranger side of Mathematics. It kept this project interesting throughout. I would also like to thank Dr. Rakesh Mohanlal for his insightful input and for reminding me to stay focused on the problem at hand.

I thank my family and friends for their support and willingness to forgive missed gatherings. In particular, I thank my parents, Pam and Sunesh Singh - for always checking in on my progress in spite of my curmudgeonly demeanour. My sisters, Priyanka Chetty and Mekara Singh for the advice, support and laughs along the way. Lastly, I thank my wife, Dr. Karishma Domah, who had to endure late nights, sinks full of coffee cups and nonsensical ramblings. Her medical expertise proved invaluable in guiding me through the complexities of the subject matter and her tenacity came in handy when my own was in short supply.

Dedication

I dedicate this dissertation to my grandmother, who wanted me to become an accountant - but is still proud nonetheless.

Abstract

This study investigates metastasis - the process characterized by cancer spreading away from the primary site and moving to secondary locations. Metastatic cancer is notoriously difficult to treat and typically results in death. Some of this difficulty stems from the mystery surrounding metastasis. The model constructed in this dissertation aims to elucidate the process with mathematical methods. Given some primary site, the model intends to predict the secondary metastatic sites. Furthermore, the model explores the relationship between metastasis and blood flow and between metastasis and the diffusive behaviour of cancer. To model cancer, various techniques across different mathematical disciplines were used. Continuum techniques model the growth and local spread of cancer. A graph network represents the organs and the blood vessels between them. Differential equations and simulation procedures govern blood flow between organs and through the vessels. An analysis of the model predictions showed a good correlation with clinical data for some cancer types. Particularly for cancers originating in the gut. The model also predicted an inverse relationship between blood velocity and the concentration of cancer cells in secondary organs. Finally, for particular diffusive behaviour, a slowing effect was observed. The investigation yields some valuable results for clinical practitioners and researchers – as it clarifies some aspects of cancer that have hitherto been difficult to study. The model provides a good framework for studying cancer progression using patient and cancer-specific information when simulating metastasis.

Contents

1 Introduction and Background **3**

1.1 Introduction 3

1.2 Biological Context 8

1.2.1 Cancer biology 8

1.2.2 Invasion Metastasis Cascade 10

1.2.3 Other Factors Influencing Metastasis 11

1.3 Literature Review 13

1.3.1 Early One-Dimensional Growth Models 13

1.3.2 Two-Dimensional Spatial Models 14

1.3.3 Metastasis Models 15

2 Methodologies and Mathematical Preliminaries **24**

2.1 Mathematical Background 24

2.1.1 Network Science 25

2.1.2 Diffusion on Networks 28

2.1.3 Advection on Networks 29

2.1.4 Hybrid and Multi-scale Modelling 30

3 Governing Equations and Numerical Methods **33**

3.1 Cancer Model 34

3.2 Advection Decay Equation 35

3.3 Numerical Simulation of Equations 36

3.3.1 Numerical Scheme Applied to Cancer Model 36

3.3.2 Numerical Scheme Applied to Advection Equation . . . 39

3.4 Simulating Cancer on One Location 40

4 Network Based Modelling **43**

4.1 Revision of Model 43

4.2 Adaption to network architecture 43

4.3 Transport through the vasculature 47

4.3.1 Intravasation 47

4.3.2 Vascular Transport 48

4.3.3 Extravasation 51

5 Results and Discussion **56**

5.1 Simulation Output and Comparison against Clinical Data . . . 56

5.2 Varying Blood Velocity 69

5.3 Varying Diffusive Conditions 73

6 Conclusion **79**

Chapter 1

Introduction and Background

1.1 Introduction

Cancer is an illness that causes a loss of tissue homeostasis resulting in seemingly, uncontrollable cellular proliferation [46]. This disease is one of the leading causes of death worldwide. The global cancer burden stands at 19.3 million new cases, and almost 10 million deaths in 2020 [22]. Estimates show that around 90% of all cancer-related deaths occur due to metastasis [85] — a process characterised by the development of secondary tumours in regions away from the primary tumour. There are limited prediction and treatment capabilities for metastatic cancer because the process is a complex interplay between numerous physiological factors [66]. This research attempts to elucidate aspects of metastasis by employing a network-based framework. This chapter serves as an introduction to the field of mathematical oncology. We first provide a background of the area, followed by the problem under investigation. After that, we discuss the aims, objectives and research questions. Finally, we conclude with the significance and limitations of this research.

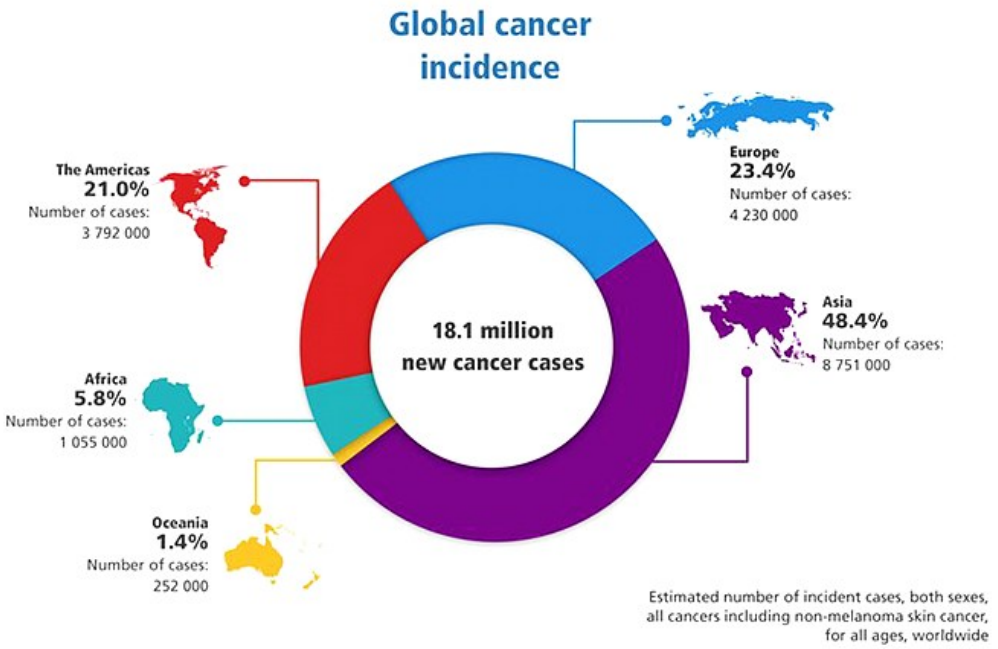

Figure 1.1: Global cancer statistics for the year 2018. Graphic by the WHO's International Agency for Research on Cancer retrieved from http://www.thepanamanews.com, accessed 2 April 2019.

Mathematical modelling techniques can help us better understand the processes of cellular proliferation, metastasis and other related phenomena by abstracting the methods underlying the development of cancer. Insights obtained from these models may prove beneficial as many aspects of cancer, such as tumour growth and spread, can be challenging to monitor [46].

There are various models in the literature for different components of cancer spread. These can range from one-dimensional differential equations which model tumour growth to hybrid simulations that model the local spread of cancer. For the one dimensional case, the early work pioneered by Benjamin Gompertz and Ludwig von Bertalanffy in [31], and [83], respectively, is of particular interest. These produce a mathematical definition of tumour growth that modern approaches still employ; hence we explore these in future chapters. After that, we highlight two-dimensional models that laid the foundation for modelling metastasis. We consider an initial attempt at Spatio-temporal modelling by Gatenby et al. [29]. Then, an effort to expand these principles to include different methods of cancer cell diffusion by Peru et al. [11]. After that, we examine a seminal model by Anderson et al. [3]

that factors in more of the histological facets of cancer. These examples all consider the spatial expansion of a growing tumour in two dimensions as it progresses through the primary organ.

To conclude our review of two-dimensional models, we study an early attempt at hybrid modelling by Vito et al. [66]. We then turn our attention to relevant models of local metastasis, such as the initial work by Saidel, Liotta and Kleinerman [71]. These introduce the concept of modelling cancer spread within the primary site, with some models investigating secondary metastasis. Next, we present a view of various pertinent metastasis models, with specific emphasis on the work of Enderling et al. [21] and Frannsen et al. [26], as these inform the work conducted in this study and, in the case of [26], represent the most explicit attempt at modelling the spread of cancer to secondary sites using hybrid simulation techniques. Some atypical models are considered, for example, computational [12] and Markov chain models [47; 57; 56], thus providing a holistic view of the current modelling environment.

The process of cancer growth and spread is a complex, multistep procedure. There are many models for the progression of tumours and the local spread of cancer cells. These provide helpful insight into the underlying dynamics of the steps in this process. However, models of secondary metastasis are still in their infancy - with very few explicitly catering for distant locations. Models that cater for this complexity can elucidate the process of metastasis for physicians and lead to better prediction capabilities for metastatic cancer. A better understanding of metastasis may lead to more optimised treatment, whilst improved predictive capabilities can provide more realistic outlooks to patients. It is therefore crucial that we further investigate metastatic models.

Given the scarcity of such models, this study aims to develop a framework capable of modelling metastasis in a spatially exact manner that can help clarify aspects of metastasis. Our objectives for this research are:

- To create a framework based on network methodologies capable of modelling the spread of cancer between primary and secondary locations.
- To evaluate this model against clinical data.
- To use the findings from the model to draw inferences about metastasis.

In achieving the above-listed objectives, we aim to answer the following questions about the process of metastasis:

- What is the most likely sequence of secondary locations given a primary tumour location?
- How does the rate of blood flow impact the process of metastasis?
- What global effect does differing the diffusive behaviour of cancer cells have on the overall spread?

The research conducted in this dissertation aims to extend the existing body of mathematical oncology by providing a framework for modelling metastasis. Currently, very few models account for the spread to secondary locations. We address this shortage by providing a method that generically models metastasis. The technique can determine likely secondary sites based on any primary site covered in the study.

Throughout the course of this research, we encountered some significant limitations. Here we briefly describe these limitations and the steps taken to subvert them where possible.

- Lack of available and consistent data: one of the intricacies of treating metastasis is the lack of data about the process. This unavailability is partly because very few patients opt to forgo treatment. It is also difficult to detect cancer early as symptoms can be mild. Some patients only notice symptoms of cancer after metastasis. As such, data is scarce for cancer that has been detected early and not exposed to corrective treatment. It is also difficult to measure the underlying histological processes for some research questions we attempt to answer, such as the blood velocity. To partially mitigate these concerns, we have used the metastasis data available to test the model's applicability, and when determining the value of various constants, we use the most biologically appropriate values available.
- Computational cost: the method introduced in this research requires significant computational resources to execute. The hybrid model uses simulation methods to capture some behaviour alongside differential techniques. As such, there are simulation procedures and numerical schemes using resources. Furthermore, the system is multi-scale in nature, as we focus on both the dynamics of metastasis at the cellular level and the global behaviour. We use smaller grid sizes for the numerical schemes to account for this. Furthermore, we run relatively fewer iterations. While this does impact our accuracy, this still allows us to study the system's global behaviour.

- Appropriateness of assumptions: some assumptions may not be biologically appropriate. We used parameters that preserved the governing equations' stability when we could not source data to determine certain biological constants.

- Consideration of histological factors: cancer is a complex process with significant steps occurring at different scales. We omit some of these steps for computational simplicity and to avoid introducing unnecessary complexity into the model. Some of the considerations we bypass include the effect of the immune response to cancer in the bloodstream, the ability of cancer cells to travel in clusters in the blood, some factors influencing metastasis (which we explore in further chapters) and some organ-level dynamics, like the unique physiological conditions at each organ. This list is not exhaustive, but it does indicate the types of processes we did not consider. We have instead focused on the core components of metastasis. We use the model to determine how these core components answer the above research questions.

In this section, we have discussed the significance of the topic under study. A brief overview of the research environment was provided. We then discussed the aims, objectives, and research questions and concluded with some of the limitations of our proposed approach. In subsequent sections, we review the biological basis of cancer and conduct an in-depth study of the approaches used to model cancer.

1.2 Biological Context

The focus of this study is the metastatic spread of cancer between organs on a vascular network. A review of the underlying biological processes that govern this phenomenon follows. Of particular interest is the invasion-metastasis cascade. This sequence refers to the ordered chain of events required for metastasis to occur [90].

1.2.1 Cancer biology

Human tissue is composed of cells, most of which contain the genomic information of the entire organism; this allows for continuous cellular repair and reproduction. Occasionally, a cell may access unnecessary information for the tasks mentioned above. This aberration may alter the proliferation rate of the cell and hence form a tumour through uncontrolled cellular proliferation [87].

These aberrations are typically the result of mutations. The underlying cause of mutations is primarily genetics [82]. However, they can also occur because of exposure to mutagens in the environment [5], for example, ultra-violet radiation, which causes skin cancer [32]. One of the most significant risk factors for cancer is advanced age. Cancer incidence increases exponentially with age. The multi-hit hypothesis seeks to explain this phenomenon. The theory states that when a cell mutates due to genetic or environmental reasons, the cell's progeny needs to undergo several additional mutations (known as hits) before a cancerous tumour can form [82]. It takes time for these hits to occur, and since an individual requires 6 or 7 hits before cancer arises, a person likely accumulates hits gradually throughout their lifespan. For example, a person may develop a benign tumour at a younger age. The tumour cells' offspring could mutate later, so the new cells grow faster than the parents. The mutation ultimately causes the tumour to turn malignant. We review some of the genetic mechanisms supporting the multi-hit hypothesis below.

There are many genes involved in cancer development. The genes associated with the growth of cancer are as follows [17]:

- Oncogenes: These are a class of genes that control a cells' proliferation and death rate. Therefore, they are particularly susceptible to causing cancer since they govern the mechanisms that underlie cancer growth.

Mutations on oncogenes can cause cells to proliferate at higher rates [17].

- Tumour Suppressor Genes: Tumour suppressor genes constrain cell growth. Mutations that render these genes inert may free cells from the limitations they provide, thus leading to uncontrolled proliferation [86].
- Micro-RNA Genes: Micro-RNA genes are responsible for regulating the expression of other genes. They can thus inhibit or promote the expression of genes. If a mutated micro-RNA gene promotes an oncogene or inhibits a tumour suppressor gene, it can result in tumour formation [49].

Multiple mutations must generally occur in several of these genes for tumorogenesis to take place [17]. Which further supports the multi-hit hypothesis. For this reason, it takes many years for a tumour to reach a sufficiently dangerous state. As a result, the elderly are more likely to experience cancers.

While these mechanisms facilitate tumorigenesis, further steps are needed for the tumour to evolve into cancer. Hanahan and Weinberg outline these steps in [33]. We present a summary of these steps:

1. Self-sufficient growth: the tumour can proliferate.
2. Insensitivity to growth suppression: the existing controls to mitigate proliferation are rendered inert.
3. Evasion of apoptosis: cells do not die off as quickly.
4. Limitless replicative potential: no factors limit cell growth.
5. Procurement of blood vessels via angiogenesis: once a tumour reaches a significant size, it requires a blood supply to provide it with oxygen and nutrients. The formation of this vascular network is known as angiogenesis [58].
6. Acquisition of metastatic properties: the tumour assumes the necessary characteristics for metastasis to occur.

Mutations on the genes listed above allow points 1-4 to occur. We summarise the process of angiogenesis and the metastatic cascade in the proceeding section.

1.2.2 Invasion Metastasis Cascade

An estimated 40% of metastasis spreads via the blood vessels; so-called hematogenous metastasis [25]. The invasion-metastasis cascade refers to the sequence of events that precede hematogenous metastasis. For a tumour to metastasise, it must first produce blood vessels via angiogenesis. We begin with a brief explanation of how tumours interact with their surrounding medium—thus enabling us to explore metastasis in greater depth.

Tumours begin when epithelial cells start to proliferate. As they grow, the tumour invades the layer directly underneath the epithelial cells, the so-called basal lamina. The cancer cells then migrate through the extra-cellular matrix (ECM), the connective tissue between cells. The cancer cells release special enzymes to degrade the matrix and facilitate migration, these are generally called matrix degrading enzymes (MDEs). The tumour releases growth factors that aid in developing new blood vessels and capillaries. The newly formed blood vessels connect to existing vascular structures to supply the tumour with blood; this also provides the tumour with an opportunity to enter the bloodstream, as the new vasculature is often "leaky". Material from the tumour can thus enter by flowing into these structures [15].

The steps in the invasion-metastasis cascade are [80]:

- Local invasion: Local invasion refers to the process whereby cancer cells detach from the primary tumour and invade the surrounding ECM. From here, the tumour cells can enter the bloodstream.
- Intravasation: Intravasation involves tumour cells migrating into existing vascular structures. Cancer cells can enter these vessels by passing through the vessel walls or leaky vessels formed through angiogenesis.
- Survival in circulation. Upon entering the bloodstream, the cells face several stresses. Some of these stresses include:
  - Apoptosis triggered by the loss of connection to the substrate.
  - Damage to the cell due to hemodynamic shear forces.
  - Predation by immune cells.
- Extravasation is when cancer cells exit the vascular system. Theoretically, tumour cells should colonise any other organ in the body. However, the cells usually metastasise on a small subset of organs. A

potential explanation for this is the tumours' inability to enter the micro-vessels of specific organs. If the diameter of the micro-vessels at these sites is small enough, the cells cannot enter the circulatory system of that organ. If a cell does enter these micro-vessels, it may extravasate by rupturing the vessel walls.

- Colonisation. If the cells survive in their new environment post-extravasation, they are still not guaranteed to proliferate. Tumour cells must adapt to their newfound surroundings and the host of challenges therein, such as inflammatory responses that release anti-angiogenic factors. If a tumour does manage to proliferate in the new environment and reaches a clinically detectable size, it is considered a "metastases". The tumour has successfully colonised the organ and concluded the invasion-metastasis cascade.

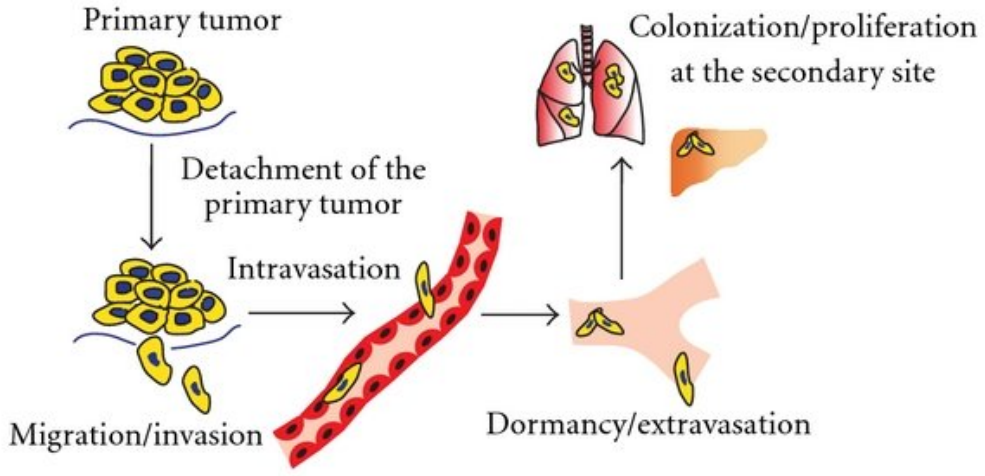

Figure 1.2: Graphical representation of the invasion metastasis cascade. Figure retrieved from [2].

1.2.3 Other Factors Influencing Metastasis

Hitherto, our focus remained on hematogenous metastasis. This section reviews other methods cancer employs when colonising distant sites. These include invasion via the lymphatic system and peritoneal spaces. Furthermore, we consider the seed and soil hypothesis - a factor that influences

metastasis beyond the items we listed in the preceding sections. These factors do not inform our model but can help us better understand where the model may deviate from clinical data.

Interstitial fluid (IF) refers to the fluid substances found between cells [89]. Lymph is a fluid derived from IF that comprises white blood cells. The IF drains into the lymphatic system via the lymph nodes. Lymph ducts transfer lymph from the nodes throughout the body. The nodes and ducts between these form the lymph network. This network is an integral component of the immune system [87]. Cancer cells can metastasise via the lymph network through various complex mechanisms beyond this study's scope. Most epithelial tumours (tumours which have developed in the epithelium - the lining of an organ) develop secondary growths through lymphatic metastasis [42]. The most common type of epithelial cancers is breast, prostate and colorectal [38].

The peritoneum is a membrane that protects the abdominal cavity. The cancers which most frequently metastasise to the peritoneum include ovarian, colorectal, pancreatic and gastric cancers, with breast and lung cancer metastasising there less often [14]. The organ is a good region for metastasis because of its sizable area and peritoneal fluid - a substance that moves in the cavity. Peritoneal fluid can harbour cancer cells from one cavity region to another [52]. Ovarian cancer metastasises via the peritoneum more frequently than other cancers, with metastasis from the gut arising less frequently but often enough to be of clinical interest [52]. Metastasis via the peritoneum can help us understand possible deviations with our observations for the gut.

English physician Stephen Paget proposed the seed and soil hypothesis [60]. Paget presented the hypothesis as a potential explanation for why disseminated cancer cells prefer specific organs. After conducting autopsies on women with fatal breast cancer, he noted a discrepancy between the organs that cancer spread to and the relative blood supply of these regions [24]. This phenomenon led him to conclude that cancers cells arising in specific organs (seeds) require a hospitable environment to proliferate (soil) [60]. Hence, cancers may favour particular metastatic sites, depending on the primary site. This proposal still holds today [23] - however; it cannot explain the metastatic patterns of all cancers [87].

This section has covered aspects of cancer that may result in deviations to the clinical data. We will use these phenomena to contextualise the findings of our model.

We have reviewed the aspects of cancer biology relevant to the research presented in this dissertation. Of particular importance is the invasion-metastasis cascade, which serves as the focus of the model constructed in the proceeding chapters.

1.3 Literature Review

This section contains a review of the relevant literature, with an initial focus on some critical one-dimensional models. Afterwards, we review some essential two-dimensional spatial models. We conclude with a detailed evaluation of applicable models of metastasis.

1.3.1 Early One-Dimensional Growth Models

Early attempts to model cancer date back to the research conducted by Benjamin Gompertz in 1825 [31]. Initially, the model did not directly describe the evolution of cancer; it has, however, been successfully fitted to tumour data [46]. This initial model assumes the form of an ordinary differential equation (ODE) whose solution represents the growth of cancer. This particular type of growth is called "Gompertzian growth". The mathematical formulation for the Gompertzian model is:

$$\frac{dV}{dt} = (a - b\ln(V))V. \tag{1.1}$$

Here V represents the volume of the growing tumour, a is the tumours proliferation rate, and b is the rate of exponential decay of the proliferation rate.

Gompertzian growth is similar to logistic growth. However, the difference lies in the former having a growth rate that exhibits flat asymptotic behaviour faster than the latter's growth rate. Therefore, one can view Gompertzian growth as a constrained logistic growth.

The work conducted by Ludwig von Bertalanffy [83] is a second example of an early cancer model. This model, similar to the Gompertz model, has as its governing equation an ODE. The equation assumes the form:

$$\frac{dW}{dt} = aW^{\frac{2}{3}} - bW. \tag{1.2}$$

In this model, W is the mass of the tumour, a is the tumour's proliferation rate, and b is the death rate of the cancer cells.

The original purpose of the model was to consider the general growth behaviour of cells by taking into account life cycles, and metabolic processes of a population of cells [30]. The advantages of both these models lie in their ability to depict the somewhat constrained nature of tumour growth (at least in the context of primary tumours), as both models describe a system with an initially exponential growth rate that is eventually limited by some asymptote. While both accurately characterise the development of a tumour, the Bertalanffy model is, on average, better suited to this particular application, possibly because Bertalanffy's model describes a biological phenomenon [30]. The standard limit of the models discussed thus far is their inability to provide a metastatic description of cancer, i.e. the spatial evolution of cancer cells [20].

1.3.2 Two-Dimensional Spatial Models

More advanced models have been constructed to address the spatial deficiency in the last few decades. These models typically materialise as partial differential equations (PDEs). Many of these models attempt to abstract the behaviour of a tumour on a cellular level. Spatial considerations are usually factored in by modelling the process of tissue invasion, which is characterised by the following properties [20]:

1. Once large enough, cancer cells escape the primary tumour and secrete various enzymes known as "matrix-degrading enzymes" (MDEs).
2. These MDEs damage the surrounding tissue or extra-cellular matrix (ECM).
3. The cancer cells begin to proliferate and migrate into the surrounding tissue.

Much of the existing literature models the complex interactions and interdependencies outlined in processes 1-3. Gatenby and Gawlinski developed an

early example of such a model [29]. They defined a system of three coupled reaction-diffusion equations describing the spatial distribution and temporal evolution of the density of healthy tissue, the density of neoplastic tissue and concentration of H^+ ions [29]. The H^+ ions interact with healthy tissue resulting in cellular degradation of the ECM, allowing for the diffusion and proliferation of cancer cells [20]. The model managed to predict the existence of a hypo-cellular gap at the interface between the normal and cancerous tissue [29]. Treatment of this interaction was extended to include haptotaxis, a process characterised by the migration of cells along the concentration gradient of another fixed group of cells [11]. Anderson et al. [3] extended these models by coupling the exact concentration of MDEs, ECM and tumour cells along with the haptotactic flux of the tumour cells along the ECM gradient.

Vito et al. [66] pursued a different approach by attempting to model tumour growth from a cellular dynamics perspective. The method employed a hybrid continuous-discrete model - using continuum methods to define chemical dynamics occurring at the tissue level and a discrete model to define individual cancer cells' interaction and migration.

Although the models of Anderson et al. [3] and Vito et al. [66] provide a more holistic view of cancer dynamics, they consider metastasis as a localised process and only account for regions close to the primary tumour. This approach is somewhat limited, as metastasis usually involves the spread of cancer to different organs.

1.3.3 Metastasis Models

Numerous models have described the growth of tumours. However, there is comparatively little effort devoted to elucidating the underlying biology of the metastatic process [6]. An early example of metastatic modelling by Saidel, Liotta and Kleinerman [71] attempts to comprehensively evaluate the haematogenous metastatic process, which is the invasion of cancer through the blood vessels [71]. Experiments were conducted by transplanting cancerous tissue into the femoral muscle of mice. The tissue was shown to have metastasised to the lungs. A lumped-parameter, deterministic model was defined, which described the evolution of the following variables with time:

1. Variable cells in the tumour.

2. Tumour vascular surface.

3. Invading tumour cells exposed on the inner vessel surface.

4. Viable tumour cells arrested in the pulmonary vessels.

5. Pulmonary metastatic sites.

Each of the processes 1-5 represents some discrete phase of the metastatic cascade. Saidel, Liotta and Kleinerman then defined a system of ODEs which they subsequently solved via Runge-Kutta numerical techniques. The model predicted the effect of various perturbations on the system. Such perturbations include tumour resection, tumour trauma, vessel growth inhibition, lung vessel damage, and inhibition of intravasation (the invasion of cancer cells into a blood vessel) [50]. The model had a good correlation with the experimental system, thus giving insight into the previously immeasurable perturbations [50].

Metastasis, like many biological processes, is stochastic. Liotta, Saidel and Kleinerman partially expanded upon the above model to include the stochastic nature of metastasis [47]. They employed a Markov Chain model that described the formation of tumour cell clumps, the phenomenon in which tumour cells travel in clumps as opposed to single cells, and the formation of colonies of cancer cells on other organs [47]. The model produced satisfactory results for the development and time evolution of metastatic sites and the time-dependent probability of finding a metastasis-free animal [50]. The study also showed that larger cell clumps would result in more aggressive metastasis formation. Therefore, breaking down these clumps could have a positive therapeutic effect [50].

Bartoszynski [7] and Hart [35], to name a few, developed further models of metastasis. These models were stochastic and provided a theoretical view of the static size distribution of metastatic colonies [41]. Iwata, Kawasaki, and Shigesada [41] later developed more dynamic models. The model proposed by Iwata et al. resulted in an equation that predicted the density of metastatic colonies for a given number of cancer cells after some time. The predicted growth rate was compared to imaging data of a patient with metastatic liver cancer (before the patient underwent treatment) to test the clinical applicability of the model. The growth rate was consistent with the patient data. The imaging data calibrated the unknown values of the model. Models defined in this manner have a specific clinical application, as imaging technology cannot detect tumours below a specific threshold; this model

would, therefore, be able to estimate the density of metastatic colonies for tumour sizes below the detectable threshold [41]. Especially relevant to this research is the model outlined by Enderling et al. in [21], and further expanded upon by Pera et al. in [64]. The model examined the impact of surgery and radiotherapy strategies on early-stage breast cancer. Similar to some of the approaches mentioned earlier, Enderling et al. formulated a system of PDEs which considers the growth and migration of cancer cells, production and diffusion of matrix-degrading enzymes and degradation of the extra-cellular matrix. The model is defined on a one-dimensional spatial domain that we denote as Ω.

The PDE governing cancer growth considers random motion and haptotaxis's impact on the growing tumour. This model is represented by:

$$\frac{\partial n}{\partial t} = \overbrace{\mu n(1 - \frac{n}{n_0} - \frac{f}{f_0})}^{proliferation} + \overbrace{D_n \nabla^2 n}^{diffusion} - \overbrace{\chi \nabla \cdot (n \nabla f)}^{haptotaxis}. \tag{1.3}$$

Where n is the number of cancer cells, μ is the proliferative rate of the cells, f is the ECM concentration, D_n is the diffusive rate of n, and χ signifies the haptotactic sensitivity coefficient.

Since cancer cells express MDEs, the production of these enzymes depends on the total concentration of cancer cells. MDEs also exhibit diffusive behaviour and will decay as the system progresses. The governing equation for MDEs is thus:

$$\frac{\partial m}{\partial t} = \overbrace{D_m \nabla^2 m}^{diffusion} + \overbrace{\zeta n(1 - \frac{m}{m_0})}^{production} - \overbrace{\omega m}^{decay}. \tag{1.4}$$

Here m is the MDE concentration, D_m refers to the diffusive rate of m, ζ is the production rate of MDEs, and ω is the decay rate.

ECM degradation is dependent on the concentration of MDEs, as these enzymes cause the deterioration of the ECM. The following equation describes this relationship:

$$\frac{\partial f}{\partial t} = \overbrace{-\kappa m f}^{degradation} \quad . \tag{1.5}$$

Where κ is the degradation rate of the ECM. The system of equations (1) - (3) exhibit zero flux boundary conditions that are represented mathematically as:

$$\begin{aligned} n \cdot \hat{v} &= 0, \\ f \cdot \hat{v} &= 0, \\ m \cdot \hat{v} &= 0. \end{aligned} \tag{1.6}$$

These conditions are defined on the boundary of Ω, which we denote as $\partial\Omega$. The term $\hat{v}$ is the outer unit normal defined on each point of $\partial\Omega$.

The variables n_0, m_0 and f_0 are biologically appropriate reference parameters for the densities or concentrations of the tumour cells, MDEs and ECM, respectively. These variables are used to non-dimensionalise the system of equations.

This model serves as a proof of principle that it is possible to create clinically testable hypotheses on the effects of radiotherapy on early breast cancer growths [21].

The model mentioned above was extended by Pera et al. in [64]. The domain is now defined as a two-dimensional square region of length L. This can correspond to a square Petri dish [64]. A diffusion tensor supplements the diffusive constant D_n, thus allowing for more varied diffusive behaviour. The tensor is given by:

$$\mathbb{D} = D_n \begin{pmatrix} a(x,y) & b(x,y) \\ b(x,y) & c(x,y) \end{pmatrix}. \tag{1.7}$$

Where a, b and c are functions of space and D_n is the diffusive constant of n. Consideration for non-standard diffusion accounts for the atypical diffusive

behaviour which some tumours exhibit. This concept will be explored further in Chapter 3.

While the earlier models adequately describe many aspects of metastasis, they do not fully account for the spread of cancer between discrete locations. Attempts to model this spread typically employ a network architecture to abstract these discrete locations. Chen et al. [12] defined one of the first models to apply network theory to metastasis. Clinical data obtained from Medicare claims were used to build a computational model. The data was based on patients aged 65 years and above and contained information regarding the primary sites of the tumour and the sequence of metastatic sites. The network topology was constructed based on this data, while an incidence hazard function determined the size of the nodes. The model could output the risk of metastatic colonies developing in other locations, given a primary location. It could also predict the most likely sequence of metastatic sites given some primary location, as well as the reverse situation [12]. While the model's accuracy was not suitable for clinical application, it conveyed the potential of network-based approaches [72].

Newton et al. [57; 56] later defined Markov Chain models with the primary aim of understanding the process rather than predicting metastatic sites. The study focused solely on lung cancer so that the resulting network was simpler to construct. The resulting organ network was fully connected, implying that cancer could metastasise from any site containing cancerous tissue to any other organ on the network. An important finding from this model was the existence of spreaders and sponges [56]. Spreaders refer to metastatic sites that increase the probability of metastatic spread, while sponges refer to sites that lower the chance of metastatic spread.

Of particular importance to this project is the work conducted by Frannsen et al. [26]. The framework defined in [26] accounts for the invasive properties of metastasis in a spatially explicit manner - this principle forms the basis of this project. What follows is an in-depth review of the model. Broadly, the model consists of a multi-grid, which represents the primary and secondary metastatic sites. Cancer cells can move and reproduce on each site. The collection of cells on each grid constitutes a cancerous growth. Consideration is given to the heterogeneous nature of these cancerous growths by accounting for two distinct cell types—namely, the more proliferative epithelial-like cells and the more invasive mesenchymal-like cells. Mesenchymal-like cells can produce MDEs. In particular, they can express *membrane-type-1 matrix metaloproteinase* (MT1-MMP), which is bound to the membrane of the

cell, and the diffusive *matrix metalloproteinase-2* (MMP-2). These enzymes result in greater invasive potential than epithelial-like cells. The individual behaviour of these cells is captured by an agent-based simulation which controls the movement, growth and metastatic spread of the cells through the vasculature. A system of PDEs accounts for ECM degradation, MDE production and diffusion, and the diffusion of cancer cells. These PDEs, coupled with the simulation, result in a hybrid discrete-continuous model which describes every step of the invasion-metastasis cascade [26].

Spatial awareness is achieved by considering $G + 1$ discrete domains. These domains correspond to the site of the primary tumour, Ω_p, and the $G \in \mathbb{N}$ potential metastatic sites, Ω_s^a, where $a = 1, 2, ..., G$. The spatial domains are discretised as a multi-grid to facilitate the agent-based simulation and the numerical solution of the PDEs.

A system of PDEs determines the motion of the cells. The density of epithelial and mesenchymal-like cells at time t and its position (x, y) on the spatial domain is expressed as $c_E(t, x, y)$ and $c_M(t, x, y)$ respectively. It is assumed that the motion of both cell types is governed by a combination of diffusion and haptotactic flux along the gradient of the ECM density, $\omega(t, x, y)$. This relationship materialises as a diffusion-haptotaxis equation and is expressed, for epithelial-like cells, as follows:

$$\frac{\partial c_E}{\partial t} = \overbrace{D_E \nabla^2 c_E}^{diffusion} - \overbrace{\Phi \nabla \cdot (c_E \nabla \omega)}^{haptotaxis}. \tag{1.8}$$

And similarly for mesenchymal cells:

$$\frac{\partial c_M}{\partial t} = D_M \nabla^2 c_M - \Phi \nabla \cdot (c_M \nabla \omega). \tag{1.9}$$

Where D_E, $D_M > 0$ is the diffusion constant for epithelial and mesenchymal-like cells, respectively. Similarly, Φ_E, $\Phi_M > 0$ is the haptotactic sensitivity coefficient for each cell type. Both equations exhibit zero-flux boundary conditions.

Mesenchymal-like cancer cells secrete diffusible MMP-2. The concentration of which, $m(t, x, y)$, is defined by the following equation:

$$\frac{\partial m}{\partial t} = \overbrace{D_m \nabla^2 m}^{diffusion} + \overbrace{\Theta c_M}^{expression} - \overbrace{\Lambda m}^{decay}, \tag{1.10}$$

along with zero-flux boundary conditions. $D_m > 0$ is the diffusive constant of the MMP-2, $\Theta > 0$ is the constant production rate of MMP-2 and $\Lambda > 0$ is the constant degradation rate of the MMP-2. The MT1-MMP enzyme is bound to the membrane of mesenchymal-like cells. Thus, mesenchymal cells determine the production, decay, and diffusion of MT1-MMP. Therefore, a separate equation for MT1-MMP is not defined.

The ECM is degraded by the MMP-2 and MT1-MMP with a rate of Γ_2, $\Gamma_1 > 0$ respectively. The evolution of the ECM is therefore determined by the following PDE:

$$\frac{\partial \omega}{\partial t} = \overbrace{-(\Gamma_1 c_M + \Gamma_2 m)\omega}^{degradation}, \tag{1.11}$$

along with zero-flux boundary conditions.

The agent-based model accounts for the proliferation of cancer cells and cell movement. Epithelial and mesenchymal-like cancer cells perform mitosis at different rates. T_E, $T_M \in \mathbb{N}$ defines the number of time steps until an epithelial-like and mesenchymal-like cell respectively performs mitosis. Epithelial cells are more proliferative than mesenchymal cells; therefore, $T_E < T_M$. A carrying capacity, $Q \in \mathbb{N}$, is defined, per grid point, to accommodate for space and resource competition. A cell will not proliferate if the grid point it inhabits is at carrying capacity. Probabilities obtained from the governing equations dictate the movement of each cell. A cell can move to all neighbouring grid points or stay in its current position.

The process of intravasation refers to the entrance of cancer cells into the vasculature. This step is crucial in the metastatic cascade, as it permits movement into secondary locations. Connectivity between the spatial domains is necessary for metastatic spread. Blood vessels are defined to rationalise this connection. Some $U_P \in \mathbb{N}_0$ healthy blood vessels and $V_P \in \mathbb{N}_0$ ruptured blood vessels are randomly distributed across the grid points. Healthy vessels

occupy a single grid point while ruptured blood vessels occupy $A^b \in \mathbb{N}$, where $b = 1, 2, ..., V_P$, adjacent grid points. Mesenchymal-like cells will successfully enter the vasculature upon landing on an entry point into a blood vessel. The cells contained in all neighbouring points will also intravasate regardless of cell type, thus permitting the movement of clusters of cancer cells. Epithelial-like cells are unable to intravasate when landing upon a standard blood vessel. Any cancer cell, regardless of cell type, will intravasate, along with all neighbouring cancer cells, if placed on a ruptured blood vessel.

Once the cancer cells, or clusters, successfully intravasate, they will remain in the vasculature for $T_v \in \mathbb{N}$ time steps, as this is representative of the biologically observed behaviour of cancer cells. Cell clusters have a probability P_d of dis-aggregating after $\frac{T_v}{2}$ time steps. Single cells and clusters of cells have a respective probability P_s and P_c of surviving after T_v time steps.

Surviving cancer cells will be placed on one of the G secondary grids, Ω_S^a with probability $\epsilon_1, \epsilon_2, ..., \epsilon_G$. The cells will extravasate through a randomly chosen blood vessel U_s^a with equal probability. If the selected grid point cannot house the cells, they will be distributed to the neighbouring grid points. If all neighbouring points have reached carrying capacity, the cells are removed from the simulation. Once the cells reach the secondary grid, they colonise the region in a manner similar to the primary grid. The model produced results which supported the evidence based hypothesis that MT1-MMP is the enzyme primarily responsible for cancer invasion.

Network models provide a valuable framework for understanding the dynamics of metastasis, which are still mostly unknown. It has particular potential in demystifying the impact of small cellular changes on the global behaviour of cancer.

In Chapter 1 of this investigation, we have introduced the topic under study. We have discussed the existing attempts to model this topic and the limitations of some of these methods. We explored the utility of our proposed model and, importantly, the model's constraints. In the subsequent sections of Chapter 1, we reviewed the biological context of cancer and metastasis in greater depth and the literature surrounding the modelling of cancer and metastasis. Chapter 2 reviews some of the necessary mathematical preliminaries and the methodologies of importance to this research. The focus of Chapter 3 is the governing equations we use to construct the simulation. Here, we also examine the behaviour of cancer on a single organ to understand how we apply this behaviour with the network architecture. After that, we derive the advection equation and adapt it to a network domain. Network

behaviour forms the basis of Chapter 4, where we describe the model in its entirety and construct the network architecture. Then we move to Chapter 5 where we test the model against existing metastasis data and analyse our research questions in the context of the model's predictions. Finally, we conclude with Chapter 6, where we reflect on the research and present some next steps for future research.

Chapter 2

Methodologies and Mathematical Preliminaries

2.1 Mathematical Background

Attempts to model biological pattern formation can be traced to Alan Turing in his seminal paper, "The Chemical Basis of Morphogenesis" [79]. He illustrates how biological patterns can arise from a homogeneous environment through chemical substances reacting and diffusing through the medium. The resulting reaction-diffusion system, while initially proposed as a model of embryonic development, was later shown to be capable of reproducing numerous spatial patterns arising in nature [44]. For example, the development of lymph nodes in zebrafish embryos [88] and, more regularly, animal skin pigmentation. Patterns formed from this system are called "Turing Patterns" and are potential explanations for self-sustained pattern formation. While this system does not consider all the nuances of a developing system, it can be helpful to describe the system qualitatively [44]. A review of methods used to define pattern formation on a network domain is conducted in the proceeding sections. First, we examine the basics of network science. After that, we explore diffusion and advection on networks. Finally, we conclude with an overview of multi-scale models, which provides a framework for coupling these concepts.

2.1.1 Network Science

A network refers to a connectedness pattern between separate entities—for example, social networks that describe how people are connected [18]. The underlying mathematical structure which characterises a network is a graph. Graphs consist of nodes, known as vertices, connected by lines, referred to as edges [8].

Definition 1. *A simple graph, G, is an ordered triple $(V(G), E(G), \phi_G)$ where V denotes the vertex set, E is the edge set, and ϕ_G is an incidence function which relates an edge to an unordered pair of vertices.*

Consider the following graph with vertex set $V(G) = \{a, b, c, d\}$, edge set $E = \{e_1, e_2, e_3, e_4\}$ and ϕ_G defined as:

- $\phi_G(e_1) = a, b$
- $\phi_G(e_2) = b, c$
- $\phi_G(e_3) = c, d$
- $\phi_G(e_4) = a, d$

The ordered triple (V, E, ϕ) produces the following graph G:

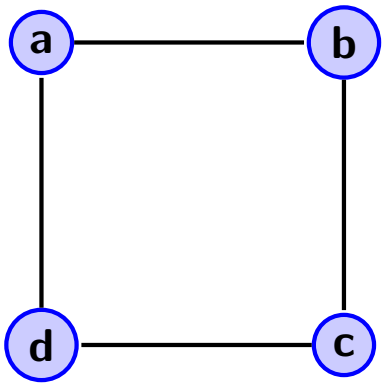

A so-called adjacency matrix is an algebraic representation of G that defines the connectivity of G.

Definition 2. *For a simple graph G, an adjacency matrix $A(G)$ is a square matrix whose indices are given by $V(G)$, that is, for each $a, b \in V(G)$, the entry A_{ab} is defined as [76]:*

$$A_{ab} = \begin{cases} 1, & a, b \in V(G) \\ 0, & otherwise. \end{cases} \tag{2.1}$$

The adjacency matrix of G is:

$$A(G) = \left[\begin{array}{c|cccc} & a & b & c & d \\ \hline a & 0 & 1 & 0 & 1 \\ b & 1 & 0 & 1 & 0 \\ c & 0 & 1 & 0 & 1 \\ d & 1 & 0 & 1 & 0 \end{array}\right] \tag{2.2}$$

We can extend the definition of a graph to cater to a broader range of physical phenomena. Of particular relevance to this study are directed and weighted graphs. We briefly describe these additional structures.

Definition 3. *A directed graph, or digraph, is a graph whose edges map to ordered pairs of vertices. In application, this graph enforces a direction in which the edge extends.*

For an edge $e_1 = a, b$, e_1 flows from vertex a to b. A consequence of this is that, unlike simple graphs, $e_1 \neq b, a$. Arrows indicate direction in visual representations of digraphs. As displayed in G_2:

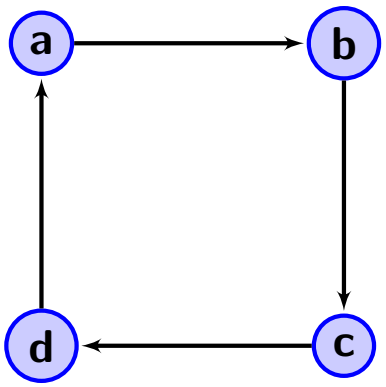

The adjacency matrix of G_2 is asymmetrical, as compared to a simple graph. Thus the adjacency matrix of G_2 is:

$$A(G_2) = \left[\begin{array}{c|cccc} & a & b & c & d \\ \hline a & 0 & 1 & 0 & 0 \\ b & 0 & 0 & 1 & 0 \\ c & 0 & 0 & 0 & 1 \\ d & 1 & 0 & 0 & 0 \end{array}\right] \tag{2.3}$$

This simple structure encapsulates many real-life scenarios. Consider, for example, road networks defined by town planners. Here, the directed edges can indicate the course of traffic flow.

Another vital feature of graphs is weighting. A weighted graph is a graph whose edges are assigned a numerical value, known as a weight. The physical interpretation of these weights is dependent on the application and can refer to any number of quantitative characteristics. Consider the previous example of a road network; the edge weights can refer to road lengths. G_3, pictured below, is an example of a weighted directed graph.

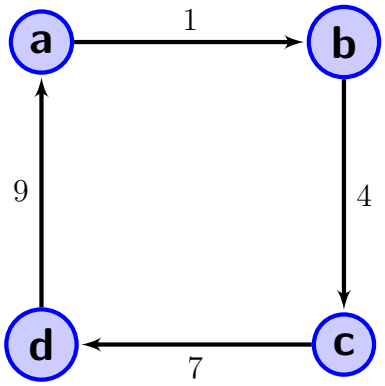

The adjacency matrix of a weighted graph stores the weight information contained in the graph. For any two connected nodes a, b on a weighted graph, the adjacency matrix at A_{ab} is the edge weight between a and b. The adjacency matrix of G_3 is thus:

$$A(G_3) = \left[\begin{array}{c|cccc} & a & b & c & d \\ \hline a & 0 & 1 & 0 & 0 \\ b & 0 & 0 & 4 & 0 \\ c & 0 & 0 & 0 & 7 \\ d & 9 & 0 & 0 & 0 \end{array}\right] \tag{2.4}$$

Graphs form the basis of network science. Network science concerns itself with the study of relationships. The difference between a graph and a network is primarily a matter of terminology. Graphs contain edges and vertices that may not be assigned a value, whereas networks consist of links and nodes with some physical interpretation. Thus, graphs are generally studied intrinsically as a mathematical structure, while a network represents existing relationships. In network science, additional mathematical techniques can aid in better-representing relationships. For example, if a substance diffuses across a network, we require a robust tool-set to model the relationship adequately. For this, we turn to continuum methods. The concept of diffusion across a network is particularly relevant to this research. We explore these concepts in greater detail in the proceeding sections.

2.1.2 Diffusion on Networks

Diffusion refers to how matter is transported from one region to another due to the random motion of molecules. Diffusion is a widespread phenomenon in biology. The applications range from cellular dynamics to epidemiological models of the spread of viruses [10]. Diffusion across networks can model a variety of phenomena not limited to Biology. For example, there are applications to statistical physics [73], information flow in social networks [92], and even the spread of dementia as it flows through different neuronal pathways [67]. Most studies examine how patterns emerge from a substance spreading across a network and the impact the network topology has on this pattern. We review the methods discussed in [4] and [36] as some of the techniques established in these studies aids in defining the cancer network.

For a directed network consisting of N nodes with the associated asymmetric adjacency matrix A, consider two interacting species (ϕ, ψ) with the concentration of these species on a node, i, given by (ϕ_i, ψ_i). A reaction-diffusion system on the network materialises as [4]:

$$\frac{d\phi_i}{dt} = f(\phi_i, \psi_i) + D_\phi \Sigma_j \Delta_{ij} \phi_j, \tag{2.5}$$

$$\frac{d\psi_i}{dt} = g(\phi_i, \psi_i) + D_\psi \Sigma_j \Delta_{ij} \psi_j. \tag{2.6}$$

D_ϕ and D_ψ are diffusion coefficients of ϕ and ψ, respectively. Furthermore, f and g are functions that govern the reaction between the species. Lastly, Δ_{ij} is the network laplacian defined as:

$$\Delta_{ij} = A_{ij} - k_i \delta_{ij}.$$

Where k_i denotes the 'outdegree' of node i, which is the number of vertices leading out of the node and δ_{ij} is Kronecker's delta. The system then gives us the change in concentration at a node by considering both the reaction between ϕ_i and ψ_i and the concentration diffusing out to neighbouring nodes and coming in from incident nodes [4].

This methodology defines a mechanism for cancer cells to traverse to distant sites via a network of blood vessels. To more suitably model the process, we must also consider the forces awaiting cancer within these vessels—for instance, the advective force of blood flow. Some forces promote apoptosis, such as shear forces. To accurately model metastasis, we must account for these features. We turn to advection processes on networks to better understand how to represent this scenario.

2.1.3 Advection on Networks

Advection and diffusion on networks go hand in hand. As a substance diffuses across a network, advective forces may act upon it. Consider cancer cells moving through a vascular network. Blood transports the cells through the vasculature. Hence the cells are driven by the velocity of the blood. We consult the framework Heaton et al. defined in [36] to capture this behaviour.

Consider a substance on a network moving between a vertex i and j - that is on edge i, j. The quantity of the resource on i, j must satisfy:

$$\frac{\partial q_{ij}}{\partial t} + R_{ij} q_{ij} + u_{ij} \frac{\partial q_{ij}}{\partial x} - D_{ij} \frac{\partial^2 q_{ij}}{\partial x^2} = 0. \tag{2.7}$$

Here x refers to the coordinates along i, j such that $0 \leq x \leq l_{ij}$, where l_{ij} is the length of i, j. The quantity of the resource per unit length is q_{ij}. The velocity of the material moving the resource is u_{ij}. D_{ij} is the dispersion co-efficient, and R_{ij} is the rate at which the resource is lost.

Equation 2.3 acts upon a one-dimensional space. For simplicity, we exclude the dispersion factor in this study. We also standardise the resource depletion rate and velocity. For our purposes, these are the death rate of circulating tumour cells and the blood velocity, respectively.

2.1.4 Hybrid and Multi-scale Modelling

The underlying behaviour of cancer contains both discrete and continuous phenomena. Cellular dynamics are best represented by discrete techniques, while other aspects, such as the changing concentration of the ECM, are more appropriately modelled by continuum methods. We must therefore consider hybrid approaches which cater to both elements. The disease typically operates on multiple time and space scales, adding to the complexity. For example, genetic mutations act on a sub-cellular level, yet the impacts occur on the cellular and tissue levels [68].

Hybrid models apply both continuous and discrete techniques to model natural processes. Discrete methods usually involve agent-based models and other cellular automata. Conversely, continuum approaches generally involve ordinary or partial differential equations. Typically, there is some degree of feedback between these paradigms. To demonstrate this, consider the model created by Frannsen et al. [26]. A discrete agent-based model governs cellular growth, reproduction, and death. The simulation yields the overall number of cancer cells on the organ, which then informs the PDE that controls the large scale migration of cells, degradation of the ECM and expression of MDEs. These factors then bias the motion of cancer cells on the agent-based model.

In general, hybrid techniques fall into two categories; off-lattice and on-lattice models. The former are models constrained to uniformly spaced grids upon which all agent interactions occur—the grid also aids in discretising the accompanying differential model. However, off-lattice models are not limited to a uniformly spaced grid and can use more realistic spatial representations of the underlying process. The focus of this study is on-lattice models. Hybrid models are often multi-scale by definition since they integrate different time

and space scales [68].

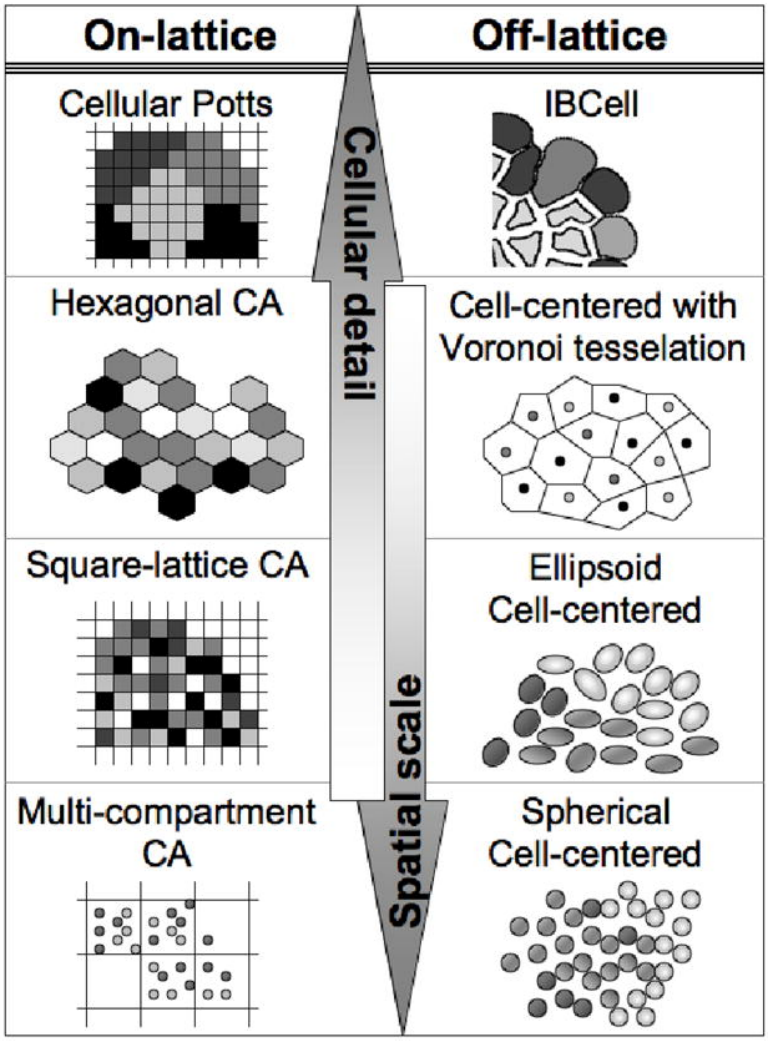

Figure 2.1: Comparison of different types of on-lattice and off-lattice models. Figure taken from [68]

The model we define in this study combines the reviewed concepts to capture the dynamics of metastasis. Network science assists us in creating a mathematical representation of the vasculature. A hybrid multi-scale model governs the dynamics of cancer on an organ level. Concurrently, the framework for diffusion across a network renders the process of intravasation and extravasation. The models for advection captures the mechanics of circulating tumour cells.

In this section, we have reviewed some of the relevant mathematical tools for constructing our model. Beginning with some elementary network models, then covering diffusion and advection on networks and concluding with a review of multi-scale models. In the proceeding section, we define the governing equations which we use for the model.

Chapter 3

Governing Equations and Numerical Methods

This section provides an overview of the models that govern cancer growth, the local spatial distribution, and the transport of cells through the vasculature. In the case of cancer growth and dispersion, we determine the general behaviour of cancer cells on a single organ. Regarding vascular transport, we explore the mechanics that underlie the cancer cells' motion as they flow within the bloodstream.

The models used in this investigation are constructed from the frameworks depicted in [26] and [64]. The agent-based model from [26], which was primarily responsible for the reproduction of cancer cells, is relaxed to save on computational cost. In its place, the system illustrated in [64] compensates for the growth of cancer. Using this system and its associated diffusion tensor, we can study the impact of different diffusive behaviours on metastasis.

Advection-decay equations control the transport of cancer cells through the vascular network. The cells move in accordance with the velocity of blood in that particular vessel. Since the cell is robbed of the nutrients it would typically obtain from the surrounding organ and is exposed to shear stress in the bloodstream, it is prone to decay - hence the inclusion of a decay term. Here we derive the equation and adapt it to a network architecture.

3.1 Cancer Model

We consider the model defined by Enderling et al. [21] and later expanded upon by Pera et al. [64]. The model, which we reviewed in Chapter 1, is reproduced to simulate organ-level dynamics of a growing tumour. The non-dimensional form of the equation is expressed as:

$$\frac{\partial n}{\partial t} = \overbrace{\mu n(1-n-f)}^{proliferation} + \overbrace{\mathbb{D}\nabla^2 n}^{diffusion} - \overbrace{\chi\nabla\cdot(n\nabla f)}^{haptotaxis}, \tag{3.1}$$

$$\frac{\partial m}{\partial t} = \overbrace{D_m\nabla^2 m}^{diffusion} + \overbrace{\zeta n(1-m)}^{production} - \overbrace{\omega m}^{decay}, \tag{3.2}$$

$$\frac{\partial f}{\partial t} = \overbrace{-\kappa m f}^{decay}. \tag{3.3}$$

Where n, m and f refer to the cancer cell, MDE and ECM concentrations respectively. The system is defined on the unit square $\Omega = (0,1)\times(0,1)$.

Notably, we have kept the diffusion tensor, $\mathbb{D}$. Including this allows us to consider the effect different diffusive behaviours have on cancer. A full breakdown of the system can be found in Chapter 1. As per the methodology in [21] and [64], we apply zero-flux boundary conditions to our solution. These conditions thus assume the same form as the boundary conditions (1.6):

$$\begin{aligned} n\cdot\hat{v} &= 0, \\ f\cdot\hat{v} &= 0, \\ m\cdot\hat{v} &= 0. \end{aligned} \tag{3.4}$$

Where $\hat{v}$ is the outer unit normal. These conditions hold on the boundary of Ω, which is defined as $\partial\Omega$. The initial conditions for the system are given by the following:

$$
\begin{aligned}
n(x, y, 0) &= N_0 e^{-\omega_0((x-0.5)^2+(y-0.5)^2)}, \\
m(x, y, 0) &= \frac{1}{2} n_0, \\
f(x, y, 0) &= 1 - \frac{1}{2} n_0.
\end{aligned} \tag{3.5}
$$

With $N_0 = 0.75$ and $\omega_0 = 0.005$, as per the values outlined by Pera et al. in [64]. These conditions allow us to create a radial tumour in the centre of the domain.

3.2 Advection Decay Equation

Blood carries the cancer cells after they enter the bloodstream. The conditions in the bloodstream differ significantly from the primary tumour site, resulting in a more hostile environment for the cells. Some factors which reduce the survival of cells within the vessels include hydrodynamic shear forces, which can tear the cell apart, and the lack of a substrate for the cell to latch onto [87].

The framework defined in [36] is applied to accommodate the situation; this entails defining an advection equation that governs the flow of particles in fluid over a network architecture. An advection equation adequately represents the transport component of this situation. A decay term is appended to the advection equation to account for the hostility of the vascular environment. The equation assumes the form:

$$
\frac{\partial n_{ij}}{\partial t} = \overbrace{v \frac{\partial n_{ij}}{\partial x}}^{Advection} - \overbrace{\alpha n_{ij}}^{Decay}. \tag{3.6}
$$

Where n_{ij} refers to the number of cancer cells in a blood vessel between node i and j, v denotes the velocity of blood and α signifies the death rate of cells in the vasculature. The domain for the equation is the one-dimensional edge i, j between nodes i and j.

3.3 Numerical Simulation of Equations

The simulation employs a hybrid strategy by programmatically handling the intravasation and extravasation mechanics. Partial differential equations govern the cell, ECM and MDE motion. This section comprises a review of the numerical techniques used to solve these equations.

3.3.1 Numerical Scheme Applied to Cancer Model

Considering the model governed by equations (3.1) - (3.3), we apply a second order central difference discretisation to approximate the spatial derivative and an explicit Euler method to calculate the time derivative. The second order central difference scheme for the spatial derivatives are stated as:

$$u_{xx} = \frac{u^k_{i+1,j} - 2u^k_{i,j} + u^k_{i-1,j}}{\Delta x^2}, \tag{3.7}$$

$$u_{yy} = \frac{u^k_{i,j+1} - 2u^k_{i,j} + u^k_{i,j-1}}{\Delta y^2}, \tag{3.8}$$

$$u_{xy} = \frac{u^k_{i+1,j+1} - u^k_{i+1,j-1} + u^k_{i-1,j+1} + u^k_{i-1,j+1}}{\Delta xy}. \tag{3.9}$$

The explicit Euler method for the time derivative is given as:

$$u_t = \frac{u^{k+1}_{i,j} - u^k_{i,j}}{\Delta t}. \tag{3.10}$$

The domain is discretised as an $\Omega = (0,1)\times(0,1)$ unit square on the Cartesian plane. A coordinate (x, y) is thus represented by $(i\Delta x, j\Delta y)$, where $i = 0, 1, ..., L_1$ and $j = 0, 1, ..., L_2$ with $L_1, L_2 \in \mathbb{N}$. Furthermore, $\Delta x, \Delta y$ denote the space steps in the x and y direction respectively. The discrete form of the time variable is $k\Delta t$, where Δt is the constant time step and $k \in \mathbb{N}$. The variables n, f and m are thus approximated at the grid points (i, j) for discrete time step $k\Delta t$ as follows,

$$
\begin{aligned}
N_{i,j}^{k} &\approx n(i\Delta x, j\Delta y, k\Delta t), \\
F_{i,j}^{k} &\approx f(i\Delta x, j\Delta y, k\Delta t), \\
M_{i,j}^{k} &\approx m(i\Delta x, j\Delta y, k\Delta t).
\end{aligned} \tag{3.11}
$$

Furthermore, the diffusion tensor assumes the following discrete form,

$$
\begin{aligned}
a_{i,j} &= a(i\Delta x, j\Delta y), \\
b_{i,j} &= b(i\Delta x, j\Delta y), \\
c_{i,j} &= c(i\Delta x, j\Delta y).
\end{aligned} \tag{3.12}
$$

We discretise the equations (3.1) - (3.2) using the derivatives outlined in equations (3.7) - (3.10) and the terms specified in (3.11) and (3.12) to obtain the following numerical scheme:

$$
\begin{aligned}
N_{i,j}^{k+1} &= N_{i,j}^{k} + a_{i,j}\frac{\Delta t}{\Delta x^2}(N_{i+1,j}^{k} - 2N_{i,j}^{k} + N_{i-1,j}^{k}) \\
&+ c_{i,j}\frac{\Delta t}{\Delta y^2}(N_{i,j+1}^{k} - 2N_{i,j}^{k} + N_{i,j-1}^{k}) \\
&+ b_{i,j}\frac{\Delta t}{2\Delta x\Delta y}(N_{i+1,j+1}^{k} - N_{i+1,j-1}^{k} - N_{i-1,j-1}^{k} + N_{i-1,j-1}^{k}) \\
&+ \frac{\Delta t}{4\Delta x^2}(a_{i+1,j} - a_{i-1,j})(N_{i+1,j}^{k} - N_{i-1,j}^{k}) \\
&+ \frac{\Delta t}{4\Delta y^2}(c_{i,j+1} - a_{i,j-1})(N_{i,j+1}^{k} - N_{i,j-1}^{k}) \\
&+ \frac{\Delta t}{4\Delta x\Delta y}[(b_{i+1,j} - b_{i-1,j})(N_{i,j+1}^{k} - N_{i,j-1}^{k}) + (b_{i,j+1} - b_{i,j-1})(N_{i+1,j}^{k} - N_{i-1,j}^{k})] \\
&+ \gamma\frac{\Delta t}{4\Delta x^2}(N_{i+1,j}^{k} - N_{i-1,j}^{k})(F_{i+1,j}^{k} - F_{i-1,j}^{k}) \\
&+ \gamma\frac{\Delta t}{4\Delta y^2}(N_{i,j+1}^{k} - N_{i,j-1}^{k})(F_{i,j+1}^{k} - F_{i,j-1}^{k}) \\
&+ \gamma\frac{\Delta t}{4\Delta x^2}N_{i,j}^{k}(F_{i+1,j}^{k} - 2F_{i}^{k} + F_{i-1,j}^{k}) \\
&+ \gamma\frac{\Delta t}{4\Delta y^2}N_{i,j}^{k}(F_{i,j+1}^{k} - 2F_{i}^{k} + F_{i,j-1}^{k}) \\
&+ \Delta t\lambda N_{i,j}^{k}(1 - N_{i,j}^{k} - F_{i,j}^{k}),
\end{aligned}
\tag{3.13}
$$

$$
F_{i,j}^{k+1} = F_{i,j}^{k}(1 - \Delta t\kappa M_{i,j}^{k}), \tag{3.14}
$$

$$
\begin{aligned}
M_{i,j}^{k+1} &= M_{i,j}^{k} + d_m\frac{\Delta t}{\Delta x^2}(M_{i+1,j}^{k} - 2M_{i,j}^{k} + M_{i-1,j}^{k}) \\
&+ d_m\frac{\Delta t}{\Delta y^2}(M_{i,j+1}^{k} - 2M_{i,j}^{k} + M_{i,j-1}^{k}) \\
&+ \Delta t\delta N_{i,j}^{k}(1 - M_{i,j}^{k}) - \Delta t\beta M_{i,j}^{k}.
\end{aligned}
\tag{3.15}
$$

The numerical scheme is selected because of its ease of implementation and because the stability of the scheme is guaranteed, provided the following upper bound on the time step, Δt, is preserved [64]:

$$
\Delta t \leq min\left\{\frac{1}{8}\frac{max(\Delta x^2, \Delta y^2)}{max_{i,j}(a_{i,j}, c_{i,j})}, \frac{1}{2}\frac{max(\Delta x^2, \Delta y^2)}{d_m}\right\}. \tag{3.16}
$$

3.3.2 Numerical Scheme Applied to Advection Equation

In order to solve equation 3.1, a first order upwind scheme is applied. This method considers the direction in which a substance is propagated through the domain. For our purposes, the substance is blood flowing through blood vessels. The scheme assumes the form:

$$\frac{u_i^{k+1} - u_i^k}{\Delta t} + a\frac{u_i^k - u_{i-1}^k}{\Delta x} = 0, \; for\, a > 0, \tag{3.17}$$

$$\frac{u_i^{k+1} - u_i^k}{\Delta t} + a\frac{u_{i-1}^k - u_i^k}{\Delta x} = 0, \; for\, a < 0. \tag{3.18}$$

The variable a represents the velocity at which blood propagates. A finite-difference stencil is used to discretise the system. When the blood flows from left to right, i.e., the velocity term in the advection-decay equation is positive, a backwards difference is used. For the opposing scenario, a forwards difference is computed instead [63]. The scheme is selected because the definition of the numerical model explicitly caters for the direction in which substances propagate [37]. The spatial domain is discretised as a one-dimensional grid of length L, where L refers to the vessel's length. The distance between grid points, denoted by Δx, is given by $\frac{L}{M}$, where M refers to the number of grid points in the domain. We can therefore define an x-coordinate on the domain as $(i\Delta x)$, where $i = 0, 1, ..., L$. As per the previous model, Δt refers to the constant time step used for the scheme. Since $v > 0$, we apply equation (3.17) to equation (3.6) and obtain the following numerical scheme [63]:

$$\frac{n_i^{m+1} - n_i^m}{\Delta t} + v\frac{n_i^m - n_{i-1}^m}{\Delta x} - \alpha n_i^m = 0. \tag{3.19}$$

We simulate equation 3.1 using this discretization by setting $M = 10$ as it provides stability and sufficient accuracy. The numerical scheme is stable provided the Courant–Friedrichs–Lewy condition (CFL) is satisfied [37]. This implies the following condition is met:

$$c = \left| v\frac{\Delta t}{\Delta x} \right| \leq 1. \tag{3.20}$$

3.4 Simulating Cancer on One Location

The domain for equations (3.1) - (3.3) is the unit square $\Omega = (0, 1) \times (0, 1)$. We discretise this as a 128×128 grid to allow for numerical simulation of the equations and, eventually, facilitate other simulation dynamics, such as extravasation through blood vessels. After running the simulation for 1000 iterations, we receive qualitatively similar results to [64] and [21]. We simulate anisotropic diffusion following the conditions stipulated in [64] and find a qualitatively good correlation with the results obtained by Pera et. al.

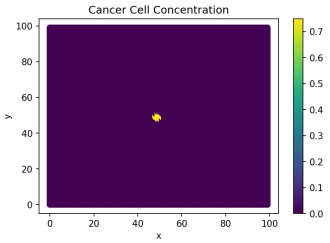

Figure 3.1: Initial Concentration of Cells

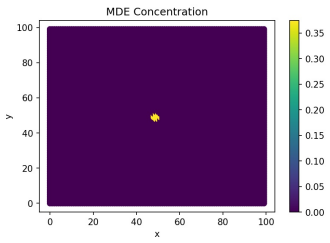

Figure 3.2: Initial Concentration of MDEs

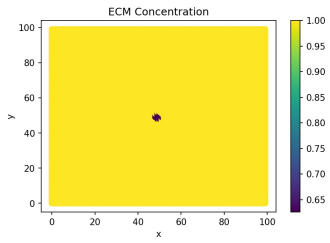

Figure 3.3: Initial Concentration of ECM

Figures 3.1 - 3.3 display the system with the prescribed initial conditions. The effect of cancer cells on MDE expression and ECM degradation is immediately apparent. The tumour is initialised as a circle at the centre of a small region of interest.

When a substance diffuses equally in all directions, we say it diffuses isotropically. When the diffusion of the substance varies with direction, it diffuses anisotropically. In the case of isotropic diffusion, the cancer cells diffuse outward in a spherically symmetrical manner. This corresponds to a diffusion tensor where $a(x, y) = 1$, $b(x, y) = 0$ and $c(x, y) = 1$. Figures 3.4 - 3.6 illustrates the case of isotropic diffusion for the three variables under study. From these figures, we note that the MDE production and cell growth and proliferation assume a directly proportional relationship. The ECM degrades in proportion to the MDE concentration.

Here, we observe good correlation with the results obtained by Pera et al. in [64]. To account for anisotropic diffusion, we set $a(x, y) = 0.01$, $b(x, y) = 0$ and $c(x, y) = 1$. This results in greater diffusion in the x direction. In particular, the cells are 10 times more diffusive in the x direction. This is visualised in 3.7.

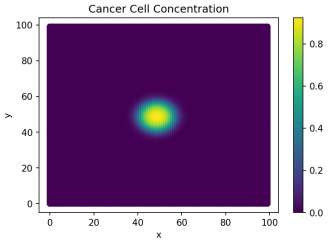

Figure 3.4: Concentration of Cells

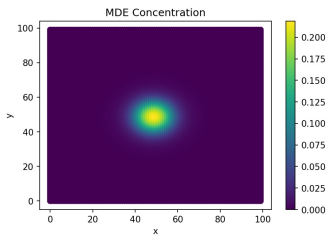

Figure 3.5: Concentration of MDEs

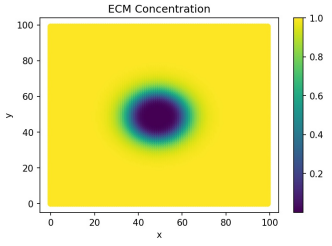

Figure 3.6: Concentration of ECM

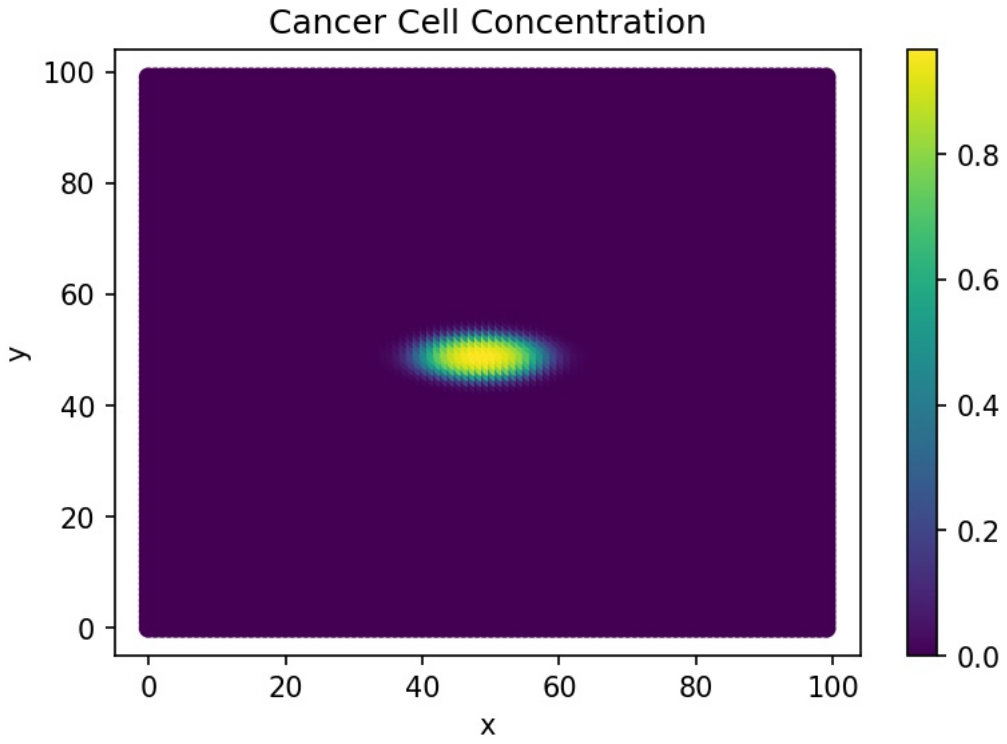

Figure 3.7: Anisotropic Diffusion

Figure 3.7 shows the qualitative difference resulting from changing the diffusive behaviour. While no explicit physiological impacts of anisotropic tumours could be obtained, we note that in certain cancers, this non-uniform diffusive behaviour results in a tumour that is significantly harder to detect with current imaging technologies [61]. In proceeding chapters, we simulate

this behaviour to understand what impact a tumour that diffuses anisotropically has on the global spread of cancer.

Chapter 4

Network Based Modelling

4.1 Revision of Model

The approach defined by Franssen et al. [26] is adapted by removing aspects of the agent-based simulation and reworking the multi-grid to fit the network approach. Moreover, we use the system of equations established by Pera et al. in [64] in place of the system outlined in [26]. We make this substitution because the model in [64] contains a source term describing the growth of cancer cells. The model also does not distinguish between epithelial and mesenchymal cells. Though we lose some robustness by removing this from the simulation, our final model will be more computationally efficient. We remove the reproductive aspect of the agent-based mode since we have a source term in the equation. More alterations to the model are presented in the proceeding sections, beginning with a review of the network methodology then moving to the travel through the vasculature. Finally, we present the numerical simulations and the complete algorithm.

4.2 Adaption to network architecture

A more traditional graph model replaces the multi-grid approach from [26], which allows for mathematical representation of complex vascular networks. Each edge of the network represents a vascular path, while each vertex signifies a potential metastatic site. For example, consider the simplified model of blood flow displayed in Figure 4.1.

Figure 4.1 is based on the system provided by Iaizzo in [39]. This system provides a view of the volume of blood the various organ systems in the body receives. The quantity of cancer cells delivered to an organ is biased in proportion to the organ's blood supply. Figure 4.1 serves as a digraph that we use to represent the vascular system. The arteries, which carry oxygenated blood from the heart, and the veins, which carry deoxygenated blood to the heart, are expressed as directed edges of varying lengths. Each vertex is weighted per the proportion of blood the organ system receives. We have excluded other locations, such as bone and skin, to focus on the major organ systems. Furthermore, these organs have more data to inform our analysis.

The digraph formed from Figure 4.1 admits the vertex set V:

$$V = \{lung, r.\,heart, l.\,heart, brain, gut, liver, kidneys\}, \tag{4.1}$$

along with the corresponding edge set E that contains all arteries and veins under study:

$$\begin{aligned} E = \{\{r.\,heart, lung\}, \{lung, l.\,heart\}, \{l.\,heart, brain\}, \\ \{l.\,heart, gut\}, \{l.\,heart, kidney\}, \{gut, liver\}, \\ \{kidney, r.\,heart\}, \{liver, r.\,heart\}, \{brain, r.\,heart\}\}. \end{aligned} \tag{4.2}$$

The following table describes the arteries and veins corresponding to the network's edges. We also provide the estimated length of the vessel. The lengths are not indicative of the actual distance between these sites, as many smaller vessels were excluded from the study. We consider the length of the main arteries and vessels used in place of a more complex vascular network. We use the length of its corresponding vessel where lengths are unavailable for a particular vein or artery. For example, we use the length of the carotid artery as an estimate for the jugular, as one is the artery that supplies the organ, and the other is the vein that takes blood away from it. We also include the cardiac outputs from Figure 4.1 as these serve as our weights for the network. The vessel length and blood velocity technically serve as weights; however, we do not consider them to maintain a clear and concise notation.

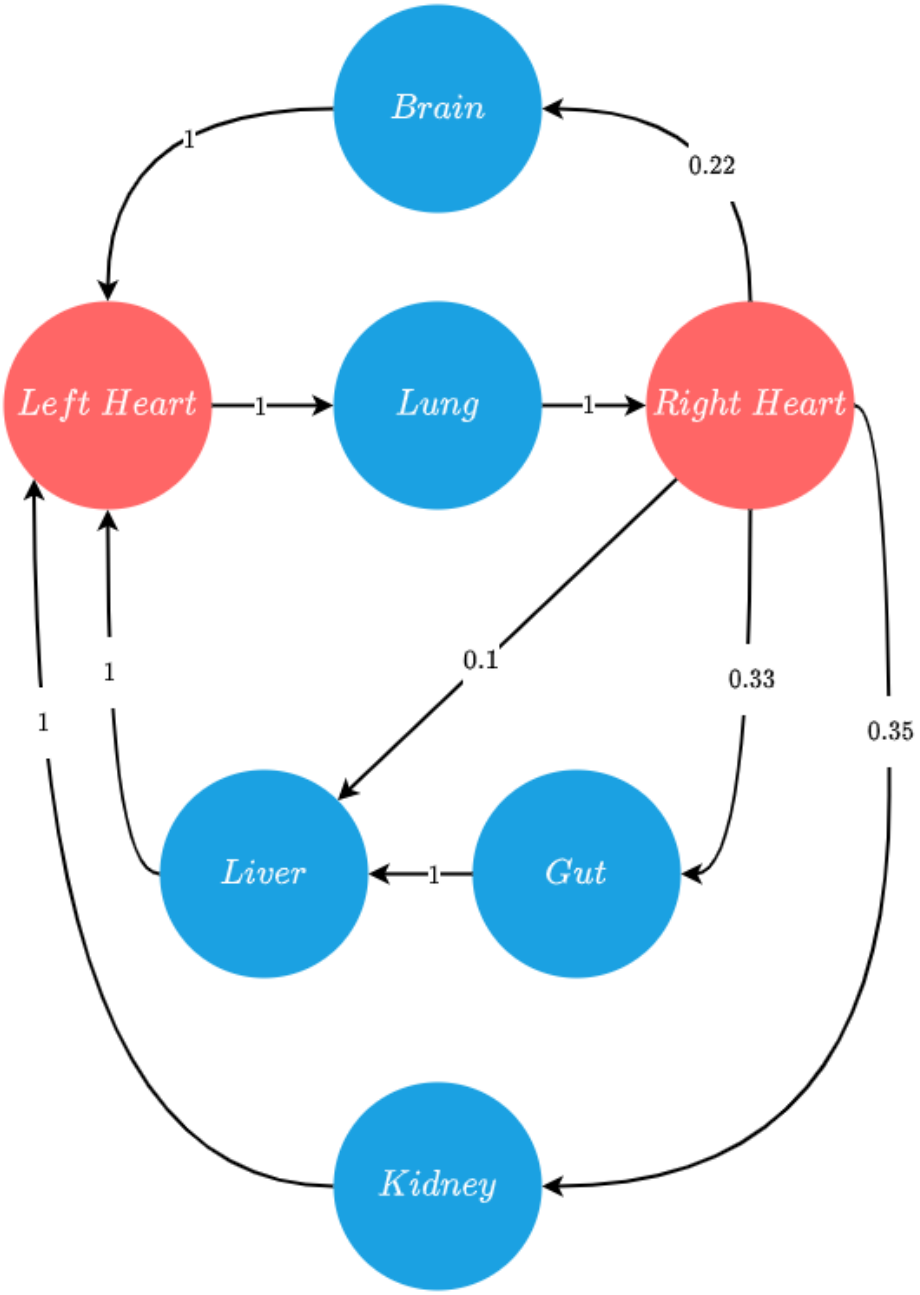

Figure 4.1: Simplified model of human circulatory system displaying cardiac output to various organ systems at a given point in time [39]

Edge	Vessel Type	Vessel Name	Cardiac Output	Vessel Length (cm)	Reference
{r. heart, lung}	Artery	Pulmonary Artery	1	5	[78]
{lung, l. heart}	Vein	Pulmonary Vein	1	5	[78]
{l. heart, brain}	Artery	Carotid	0.22	20	[13]
{l. heart, gut}	Artery	Abdominal Aorta	0.33	13	[28]
{l. heart, kidney}	Artery	Renal Artery	0.35	3	[54]
{l. heart, liver}	Artery	Hepatic Artery	0.10	6.5	[54]
{gut, liver}	Vein	Hepato Portal Vein	1	6.80	[54]
{kidney, r. heart}	Vein	Renal Vein	1	8.5	[16]
{liver, r. heart}	Vein	Hepatic Vein	1	6.80	[54]
{brain, r. heart}	Vein	Jugular	1	20	[13]

Since all the blood in each organ goes back to the heart, the cardiac output of every vein is 1.

We denote the weight of an edge between node i and j as $\gamma_{i,j}$. This weighting corresponds to the proportion of blood that the organ represented by i sends to the organ represented by j. The graph thus assumes the following adjacency matrix:

$$A = \left[\begin{array}{c|ccccccc} & lung & l.\,heart & r.\,heart & brain & gut & liver & kidney \\ \hline lung & 0 & 1 & 0 & 0 & 0 & 0 & 0 \\ l.\,heart & 0 & 0 & 0 & 0.22 & 0.33 & 0.1 & 0.35 \\ r.\,heart & 1 & 0 & 0 & 0 & 0 & 0 & 0 \\ brain & 0 & 0 & 1 & 0 & 0 & 0 & 0 \\ gut & 0 & 0 & 0 & 1 & 0 & 1 & 0 \\ liver & 0 & 0 & 1 & 0 & 0 & 0 & 0 \\ kidney & 0 & 0 & 1 & 0 & 0 & 0 & 0 \end{array}\right] \tag{4.3}$$

Adapting the system of equations defined in [64] to this domain is done by implementing the equations across all nodes. The system then takes the form:

$$\frac{\partial n_i}{\partial t} = \mu n_i(1 - \frac{n_i}{n_0} - \frac{f_i}{f_0}) + \mathbb{D}_i\nabla^2 n_i - \chi\nabla\cdot(n_i\nabla f_i), \tag{4.4}$$

$$\frac{\partial m_i}{\partial t} = D_m\nabla^2 m_i + \zeta n_i(1 - \frac{m_i}{m_0}) - \omega m_i, \tag{4.5}$$

$$\frac{\partial f_i}{\partial t} = -\kappa m_i f_i. \tag{4.6}$$

Where $i \in V$ and n_i, m_i and f_i refer to the cancer cell, MDE and ECM concentration at node i. For simplicity, the constants remain the same across all nodes. The system persists zero-flux boundary conditions as outlined in

Chapter 3. The primary node refers to the node at which cancer originates. Initial conditions at the primary node are given by the following:

$$\begin{aligned} n_0(x,y) &= N_0 e^{-\omega_0((x-0.5)^2+(y-0.5)^2)}, \\ m_0(x,y) &= \frac{1}{2} n_0, \\ f_0(x,y) &= 1 - \frac{1}{2} n_0. \end{aligned} \tag{4.7}$$

With $N_0 = 0.75$ and $\omega_0 = 0.005$. These conditions simulate the initial radial nature of the tumour. In all other nodes, $n_0 = 0$, $m_0 = 0$ and $f_0 = 1$, until some tumour cells extravasate. Each node is modelled as a 128×128 grid to allow for numerical simulation of the equations and facilitate other simulation dynamics, such as extravasation through blood vessels. This grid size was selected to maintain consistency with Pera et al. [64]. For cancer to spread to the other nodes, it must travel through a vascular section. A review of this process follows.

4.3 Transport through the vasculature

Cancer cells must enter the bloodstream or lymphatic network to colonise other organs. This study focuses solely on travel through the vascular network - the system formed by the blood vessels and organs. Once the cells intravasate, they move along with the flow of blood [87]. This section focuses on describing the process of intravasation and transport through blood vessels mathematically. Aspects of the simulation in [26] are reworked to facilitate this approach.

4.3.1 Intravasation

On each grid, eleven random points are chosen as blood vessels through which the cancer cells can exit and enter. These points represent the blood vessels tumours form when undergoing angiogenesis. For each simulation iteration, the cancer cells located on a blood vessel enter the bloodstream. The total number of cells exiting a node i is:

$$E_i = \epsilon n_i(x_b, y_b). \tag{4.8}$$

Where $n_i(x_b, y_b)$ represents the number of cells contained on a blood vessel point (x_b, y_b) on the node i and ϵ is the proportion of cells at the vessel which successfully intravasate. We set ϵ to 4.5×10^{-6}, in line with proportions observed by Yohan et. al. in [43].

4.3.2 Vascular Transport

Blood carries the cancer cells after they enter the bloodstream. The conditions in the bloodstream differ significantly from the primary tumour site, resulting in a more hostile environment for the cells. Some factors which reduce the survival of cells within the vessels include hydrodynamic shear forces and the lack of a substrate which the cell can latch onto [87].

We use the Equation (3.6) that we defined in Chapter 3. We restate the equation here so we can better understand how the newly defined constants and boundary conditions impact the equation.

$$\frac{\partial n_{ij}}{\partial t} = \overbrace{v\frac{\partial n_{ij}}{\partial x}}^{Advection} - \overbrace{\alpha n_{ij}}^{Decay}. \tag{4.9}$$

As per Chapter 3, α signifies the death rate of cells in the vasculature. We let $\alpha = 5.8 \times 10^{-6}$. This value is obtained from work conducted by Liu et al. in [48]. Here, they study the effect of hemodynamic shear stress on cancer cells in circulation. They surmise that roughly 50% of cancer cells die every 24 hours. We arrive at our chosen value by expressing this rate in seconds. The following boundary condition is prescribed:

$$n_{i,j}(0, t) = \frac{E_i}{\gamma_{i,j}}. \tag{4.10}$$

Where E_i is the above mentioned exit proportion at node i and $\gamma_{i,j}$ is the weighting of the edge between i and j. This equation implies that the number of cells leaving node i serves as the boundary condition for the transport system. Therefore, at each simulation iteration, several cells proportional to the concentration at node i will enter the bloodstream. These cells divide across all the outgoing blood vessels connected to the organ. The amount of cells each vessel receives is proportional to the volume of blood that the corresponding organ receives. This process is visualised in the following Figure.

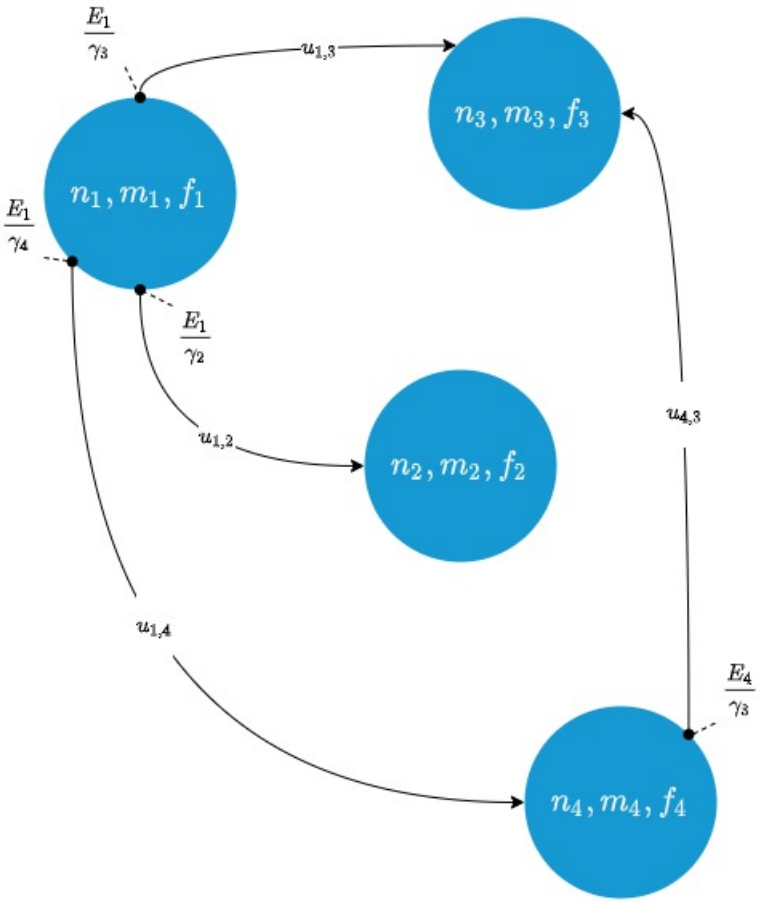

Figure 4.2: An overview of the model and how the different systems interact with each other

In Figure 4.2, we highlight one of the main contributions of this work. Here, we describe the transport dynamics along the edges through the auxiliary equation (4.9). The equation is coupled to the system of equations (4.4) - (4.6) at the vertices through the boundary conditions.

4.3.3 Extravasation

Cancer cells colonise other organs through the blood vessels. The process of extravasation can occur at all organ systems, except the left and right heart nodes. These represent chambers of the heart and are used to simulate circulatory mechanics accurately. The cells contained at the point $n_{ij}(L,t)$ are distributed into the node j on a randomly chosen blood vessel point. To accurately simulate metastatic invasion, a proportion of cells are trapped in the micro-circulation of the organ. Some of these cells are lethally damaged in this location and thus do not extravasate. The remainder stays in the circulatory system and enter the heart via the corresponding vein. A value for the proportion of cells that stay in the circulatory system could not be obtained from the literature. In this section we provide an estimation for this value.

Monte Carlo methods are well suited to solving problems involving variables that are seemingly random. Typically, a Monte Carlo simulation involves sampling a statistical distribution to generate random values for these variables. This simulated random data can be used to draw conclusions about the underlying processes. For example, Monte Carlo methods can be used to estimate unknown values, sample from random variables and optimise processes [45].

A Monte Carlo simulation was conducted to estimate the proportion of cells that remain trapped in the circulatory system, which we designate as κ. The simulation compares the diameter of the capillaries that cells pass through against the diameter of circulating tumour cells. After running this comparison for a certain number of iterations, we estimate a value for κ. Upper and lower bounds for the diameters were sourced from the relevant literature. These ranges and the associated references are visualised in the table below.

Variable	**Lower Bound (LB)**	**Upper Bound (UB)**	**Reference**
Tumour Cell Diameter (T_d)	7.2	15	[34]
Capillary Diameter (C_d)	5	10	[39]

To correctly simulate this scenario, we generate random observations for the diameter of capillaries and tumour cells using the prescribed ranges from the preceding table. Since we lack substantial empirical data for these properties, we must use estimates to obtain some of the values needed to create these observations - in particular, the mean and standard deviation of data that would fall within this range. We use the following method prescribed by Xiang et al. in [84] to arrive at this estimate:

$$\bar{X} = \frac{UB + LB}{2}, \tag{4.11}$$

$$\sigma = \frac{UB - LB}{\sqrt{12}}. \tag{4.12}$$

Where $\bar{X}$ is the mean and σ is the standard deviation. It is assumed that these values are log-normally distributed since they cannot assume a negative value. Using a log-normal random number is also more realistic than a uniform random observation, as extreme values are less likely in the log-normal case. We thus create an estimated value for the diameter of CTCs and capillaries by inverse sampling a log-normal distribution with a mean and standard deviation provided by equations (4.11) - (4.12). For each simulation iteration, a random value is generated, giving us a simulated cancer cell and capillary diameter. If the cancer cell is too large for the capillary, the cell remains in the micro-circulation of the organ. If the cell is smaller than the capillary, it passes through the organ and remains in circulation. While this method only provides a rough approximation, it does account for the large degree of variability displayed in blood vessels and tumour cell sizes whilst remaining within a reasonable range.

The simulation ran for 10000 iterations. This value is selected as it was experimentally observed that the simulation converged to our final κ value after approximately 10000 iterations. By counting the iterations which resulted in a cell passing through the capillaries and dividing by 10000, we obtain values for κ. We repeat this process 100 times to produce a distribution of κ-values; this process is visualised in Figure 4.4. In line with the observed results, κ is selected as 0.0935. This value corresponds to the average of the most common range in the distribution from Figure 4.3.

Cells trapped within the organ's micro-circulation face further stress; the cells are traumatised when stuck in these spaces as they are often too large for the region. An estimated $85\% - 95\%$ of these cells are lethally traumatized

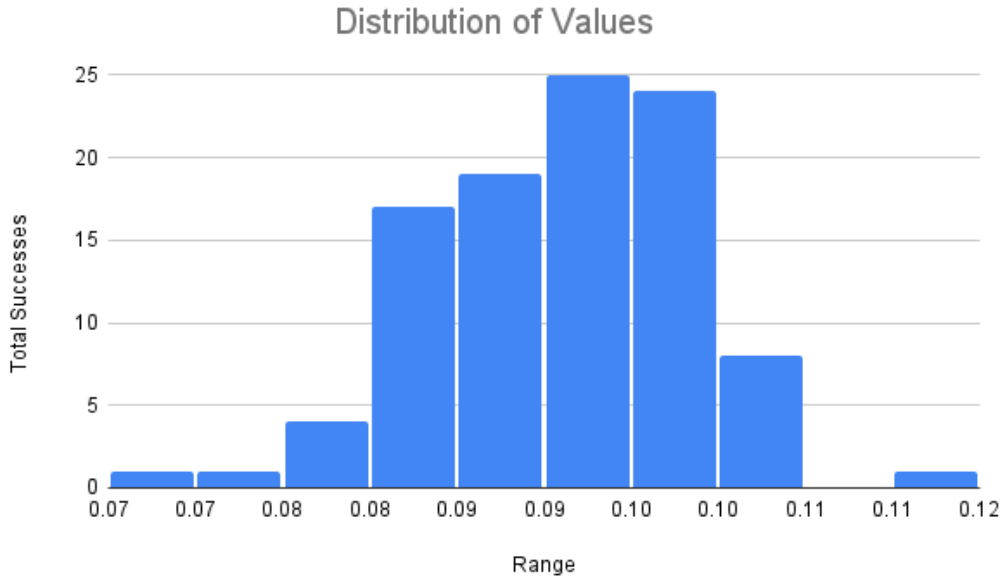

Figure 4.3: Distribution of κ-values

[59]. We cater for this by removing 90% cells stuck in the micro-circulation.

The final challenge that the cells face is adapting to the new environment. The cancer cell must proliferate in the organ to successfully colonise the region. Of the tumour cells that enter the circulation, approximately 0.01% of cells successfully form metastases [80]. We use this value to estimate the number of cells that successfully form new tumours.

Figure 4.5 summarises the simulation mechanics we have discussed thus far. This section reviewed the modification of existing models to the network architecture we have developed for this study. In the subsequent section, we discuss the results obtained from implementing this simulation.

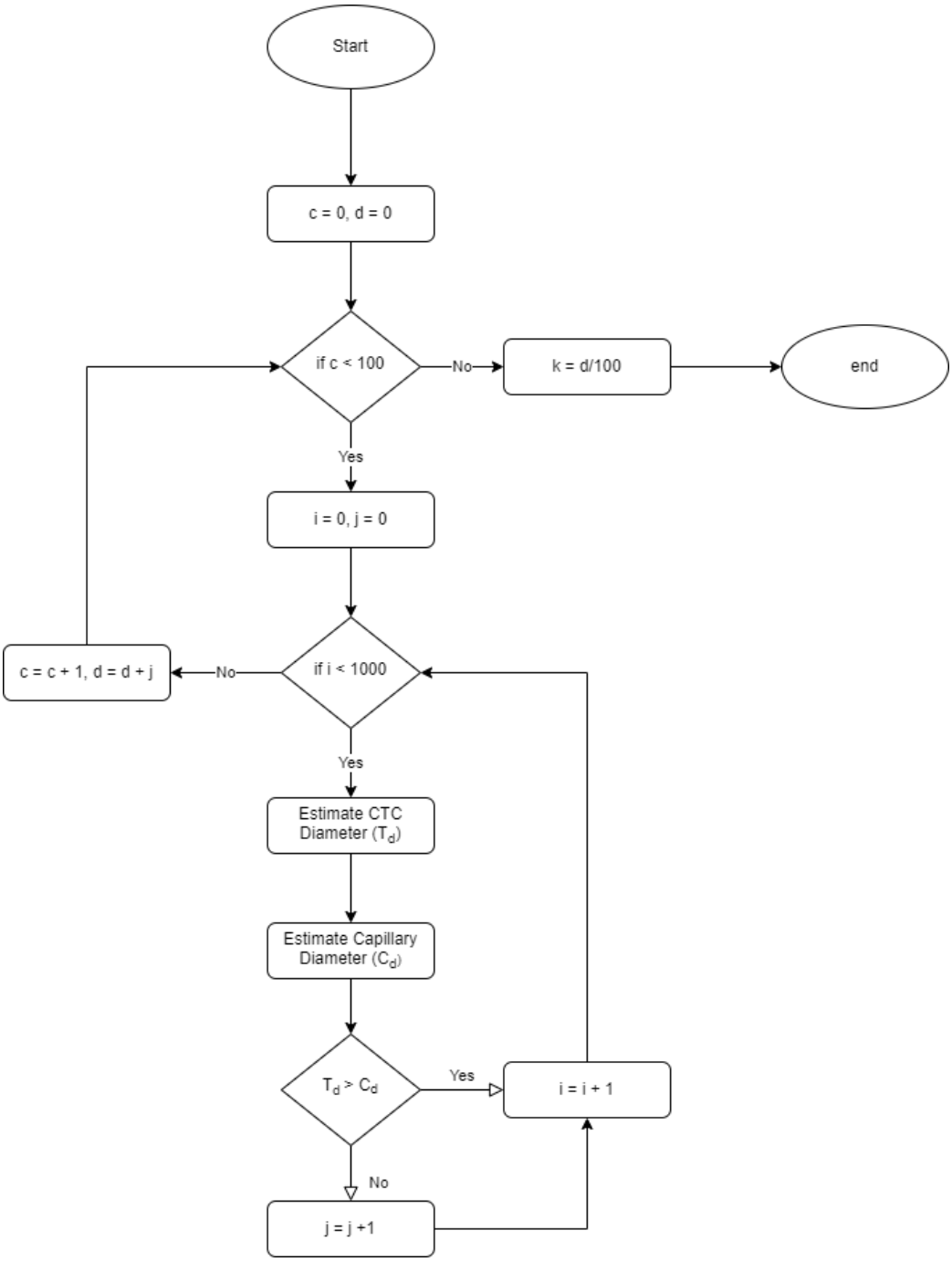

Figure 4.4: Monte Carlo Simulation Algorithm

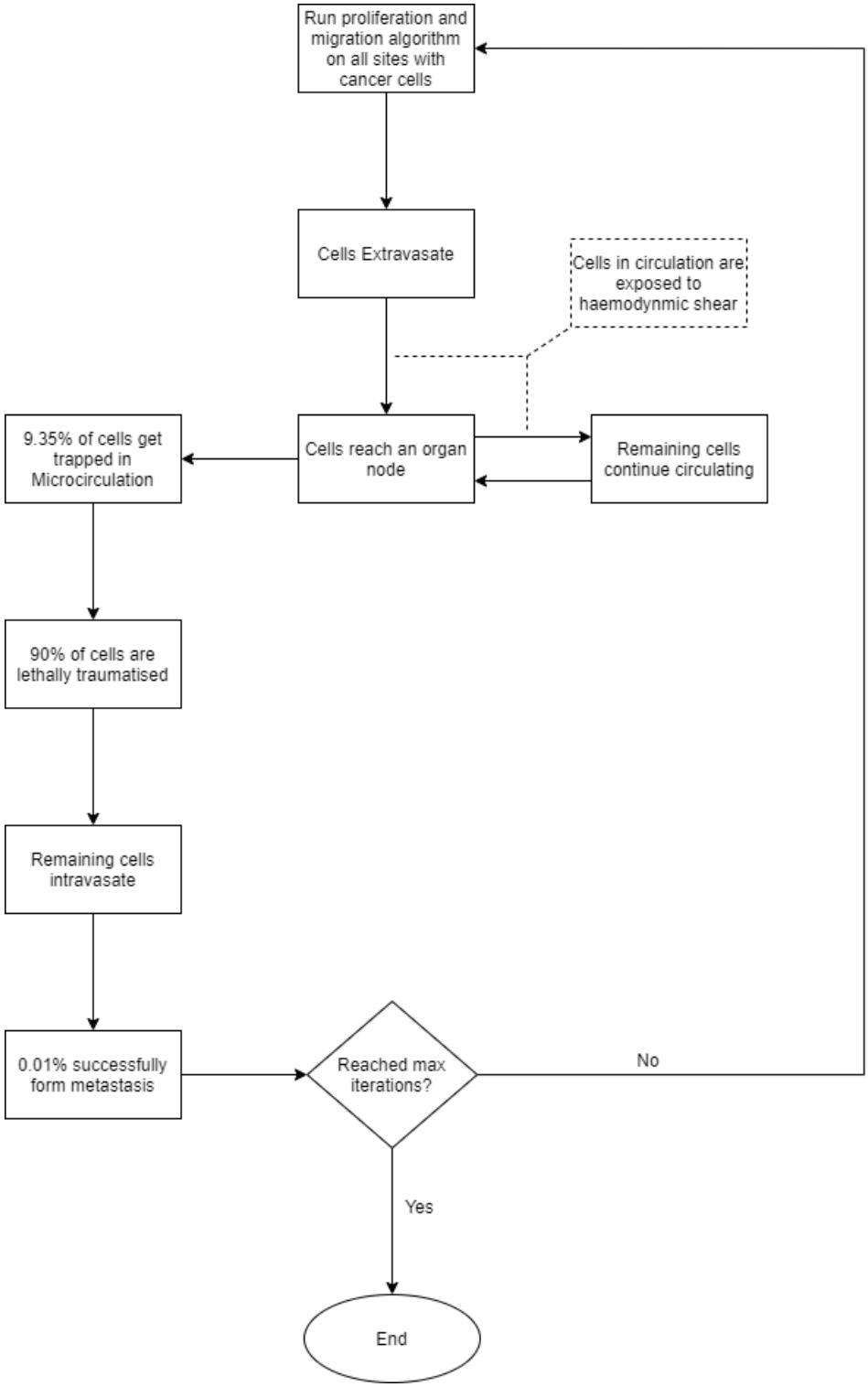

Figure 4.5: Network based simulation

Chapter 5

Results and Discussion

This section contains the results of the computational simulation and a discussion of their significance. We first determine the feasibility of the model by contrasting it with clinical metastasis data, thus allowing us to determine the metastatic routes favoured by different forms of cancer. After that, we vary the blood velocity across a biologically realistic range and analyse the impact. The analysis helps elucidate the relationship between blood velocity and metastasis. We also simulate a cancer diffusing anisotropically, this allows us to study the global effects of anisotropic diffusion.

5.1 Simulation Output and Comparison against Clinical Data

We first compare the output of the simulation against existing metastasis models. The output we receive is qualitatively similar to existing models. Cancer cells diffuse in a radially symmetric manner. We also note similar behaviour to the metastasis models established by Franssen et al. in [26]. We initiate cancer cell growth in the gut.

Figure 5.1 shows the change in the distribution of cancer cells between various iterations of the simulation. At $n = 0$, we observe the initial configuration of the simulation, as described in the preceding chapters. We note that the cells have diffused in a radially symmetrical manner at higher concentrations. The corresponding Figure 5.2 shows the distribution of cancer cells in the liver. This site is selected as it contains the highest proportion of cancer cells out-

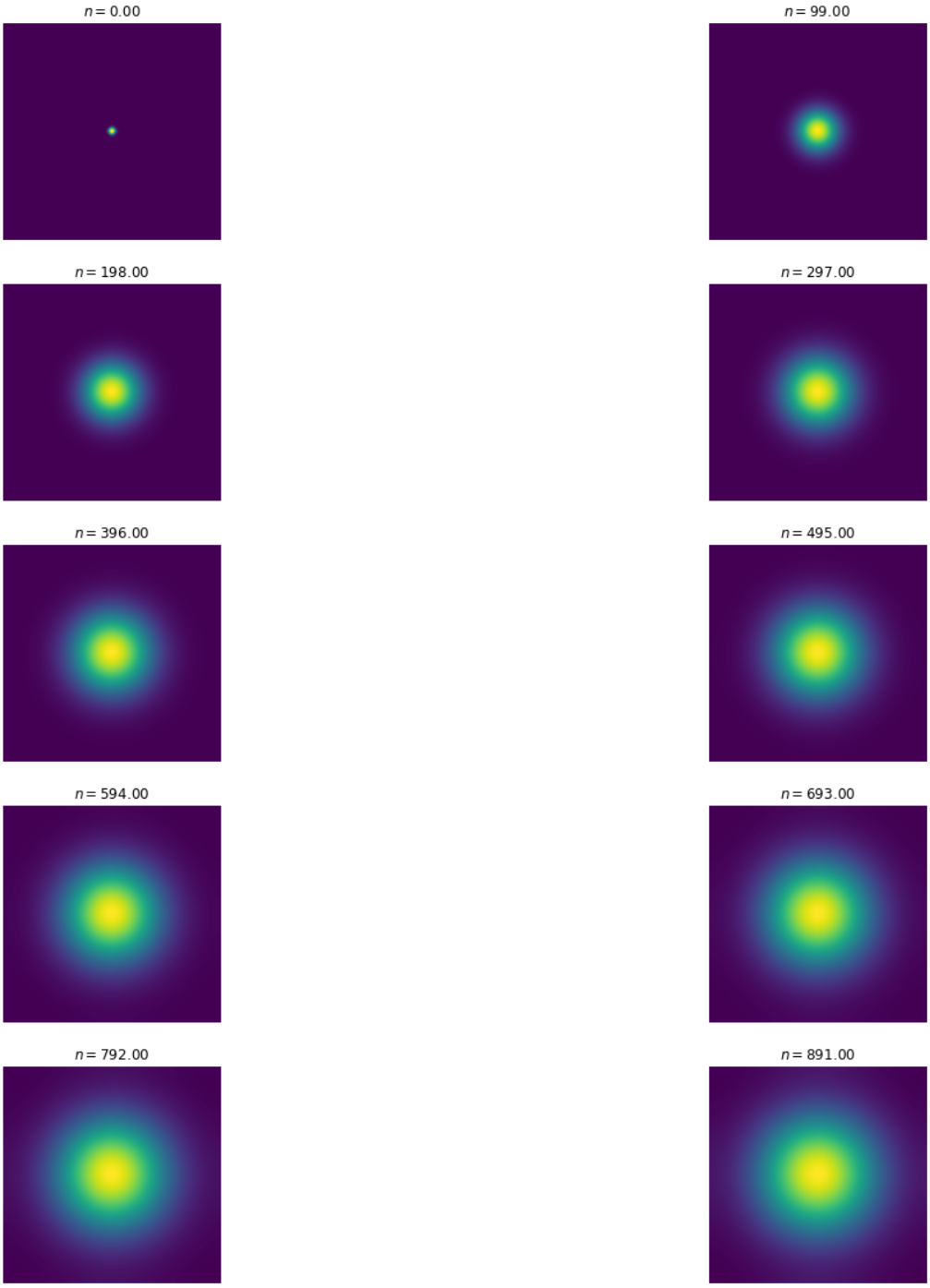

Figure 5.1: Change in Cancer Cell Distribution in Primary Site (Gut).

side of the primary site. Here we note the formation of micro-tumours as they proliferate in their new environment. We observe that the tumours increase in concentration as the simulation progresses. The high concentration of cancer cells in the liver is in line with clinical observations [81]. The finding is expected because blood from the gut must pass through the hepato-portal vein and into the liver. Since this structure is captured in the simulation, we experience similar results.

The cancer cell concentration in the gut and liver is visualised in 3-dimensions in Figure 5.3. This visualisation effectively displays the growth and diffusion of the primary tumour in the primary site and the formation of successful micro-tumours in the secondary site.

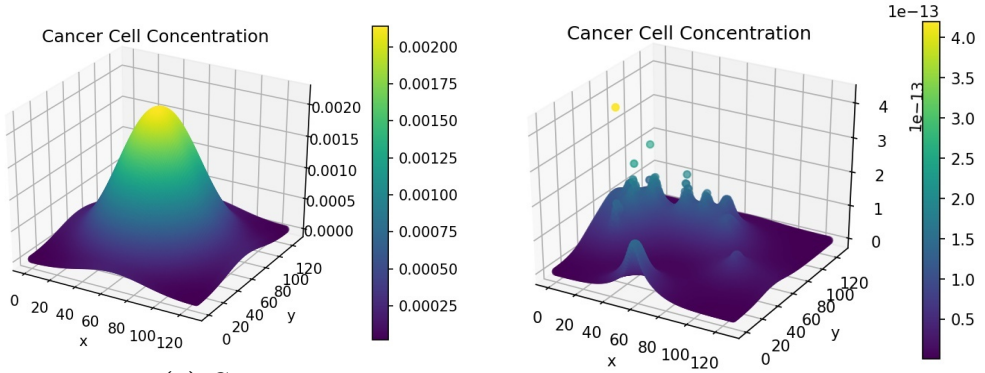

(a) Gut

(b) Liver

Figure 5.3: Cancer Cell Concentration in the Gut and Liver

Figures 5.4 and 5.5 show the ECM and MDE concentration in the gut and liver respectively. An important observation from Figure 5.3 is the small scale of the cancer cell concentration. To account for this, we first note that the growth we achieve on primary sites is qualitatively similar to the growth observed in other works, such as the work conducted by Pera et al. in [64]. The results have a smaller scale because of the metastasis dynamics we introduced, as primary sites lose some cells to extravasation. The proliferative behaviour on secondary sites is aligned to what we anticipate based on the behaviour of the primary site - particularly, conical peaks that begin to form micro-tumours as the simulation progresses. This growth is also qualitatively similar to the views from Frannsen et al. in [26]. It differs on a quantitative level because much of the dynamics in [26] was modelled using discrete techniques. For these reasons - we infer that the simulation is appropriate to explain qualitative behaviour of metastasis despite the small scale. It

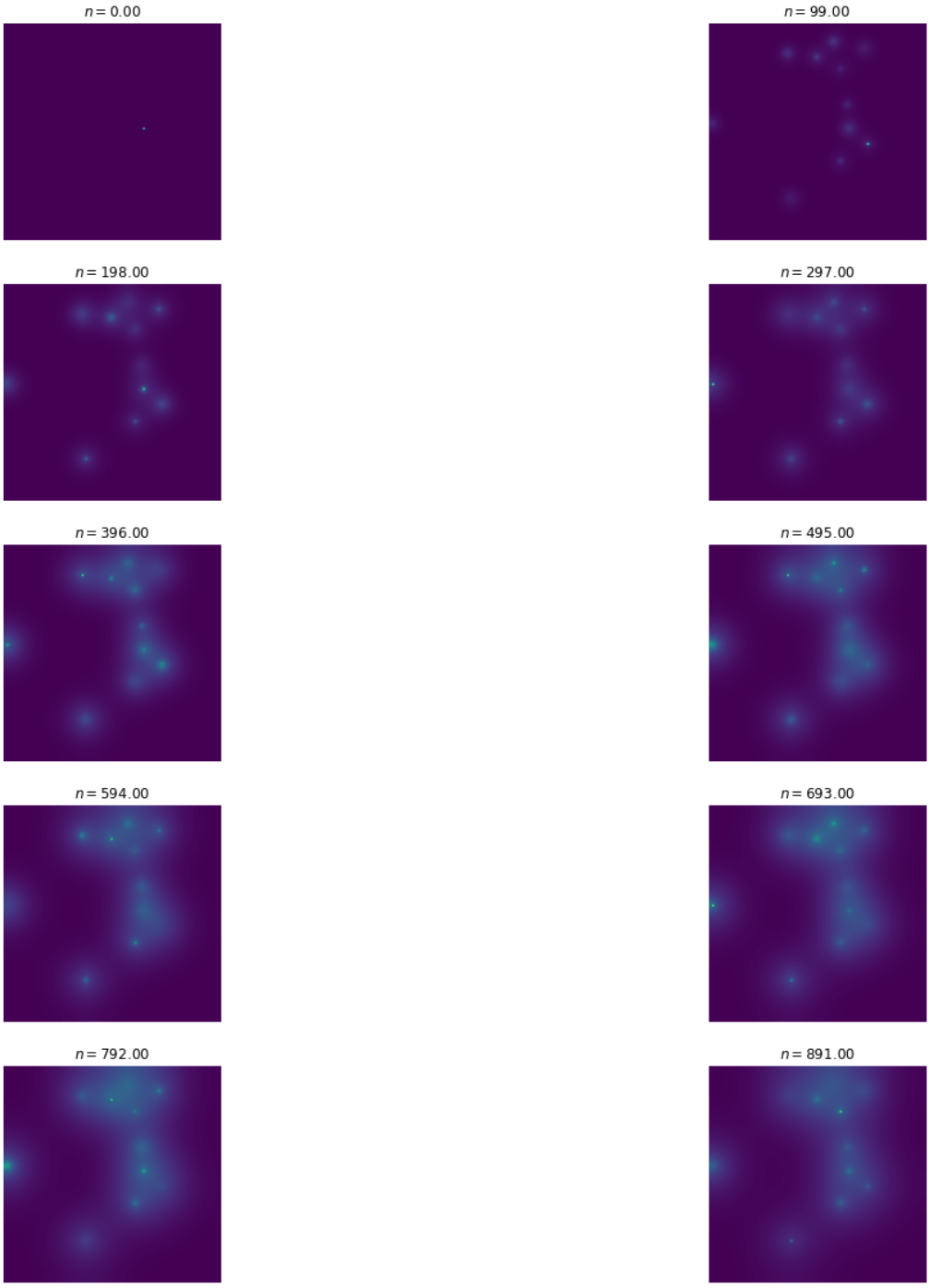

Figure 5.2: Change in Cancer Cell Distribution in Metastatic Site (Liver).

is, therefore, not used to predict exact values (like the exact concentrations of cells after a certain amount of time) - but rather to elucidate the more mechanistic aspects of metastasis; hence we express quantitative differences as proportions.

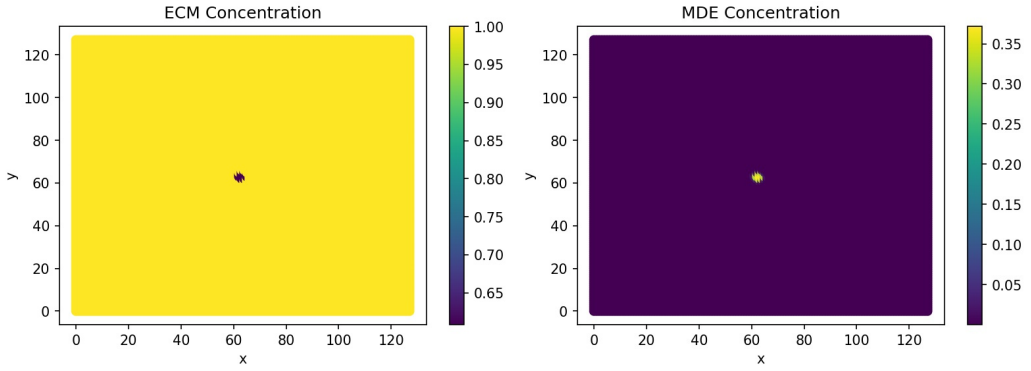

(a) ECM **(b)** MDE Concentration

Figure 5.4: ECM and MDE Concentration in the Gut after 1000 Iterations

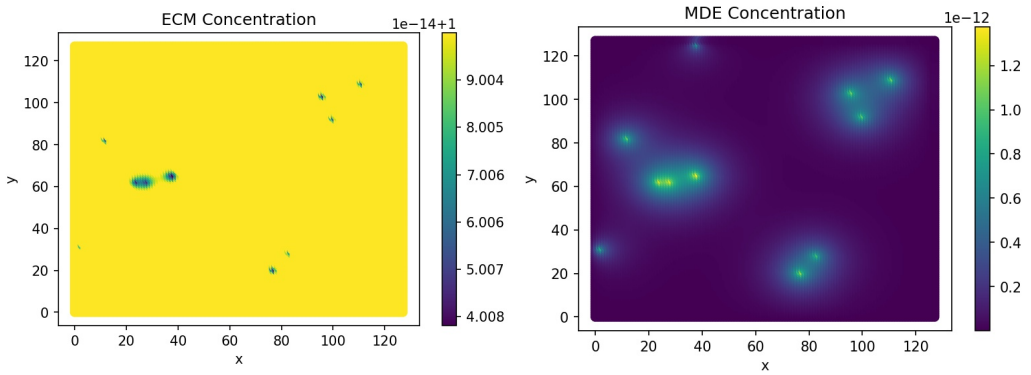

(a) ECM **(b)** MDE Concentration

Figure 5.5: ECM and MDE Concentration in the Liver after 1000 Iterations

The behaviour displayed in Figure 5.4 shows that the degradation of the ECM is aligned to the production of MDEs. We experience the most degradation in the region's centre as the cancer cells are primarily concentrated there. In Figure 5.5, the ECM and MDE degradation align with the sites of micro tumours. We note that Figure 5.5 looks dissimilar to Figure 5.2 as it was created using a different instance of the simulation.

The following series of figures shows the concentration of cancer to other organs in the system, namely, the lungs, brain and kidney. We note that each organ contains some micro-tumour development mainly because of how the model is constructed. Cells are not prevented from travelling to other locations; a small proportion migrates to other sites based on the quantity of blood arriving at the organ. However, in some organs, this value is minimal; this can be interpreted as a lower probability of metastasis.

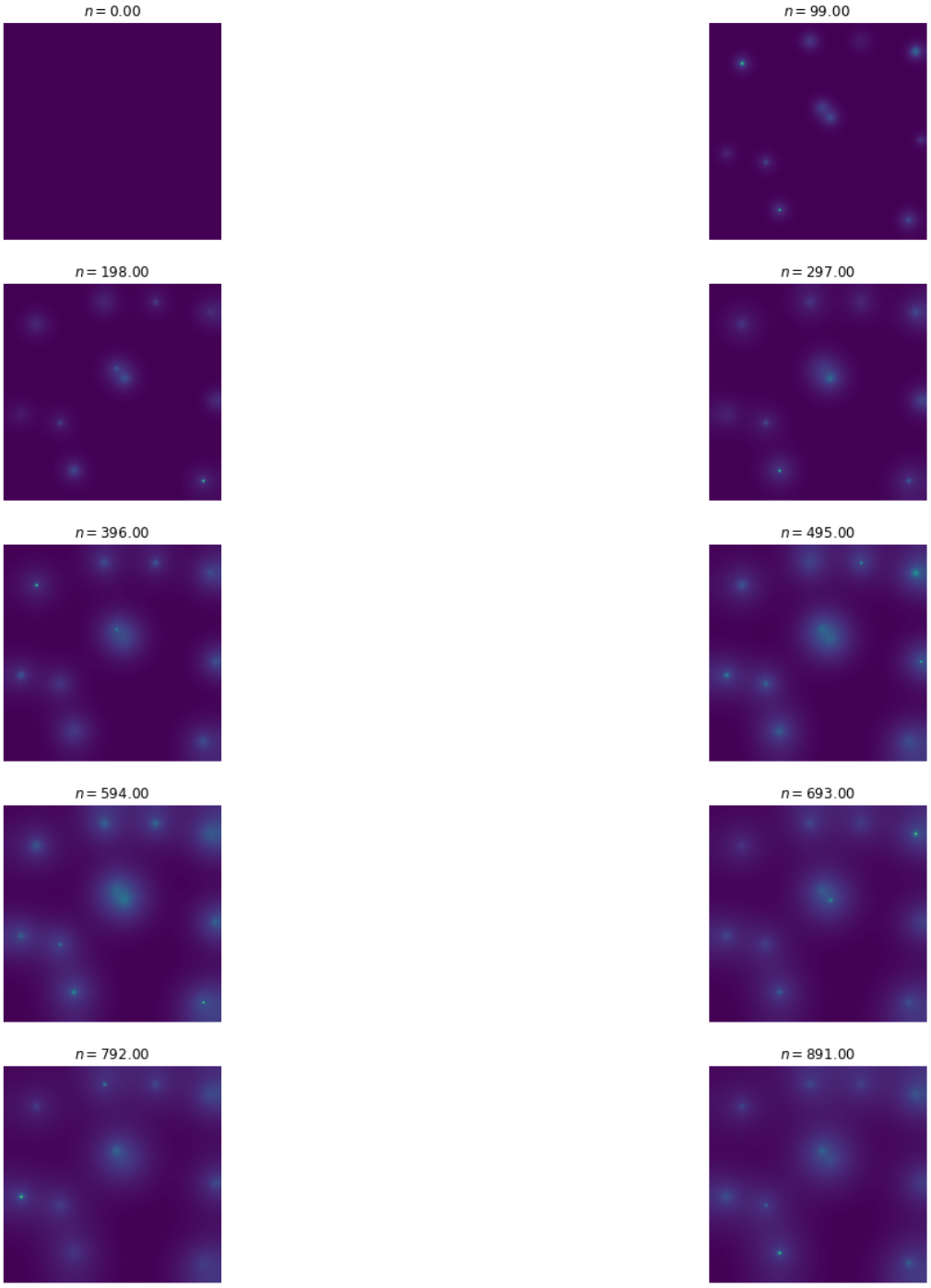

Figure 5.6: Change in Cancer Cell Distribution in Metastatic Site (Lung).

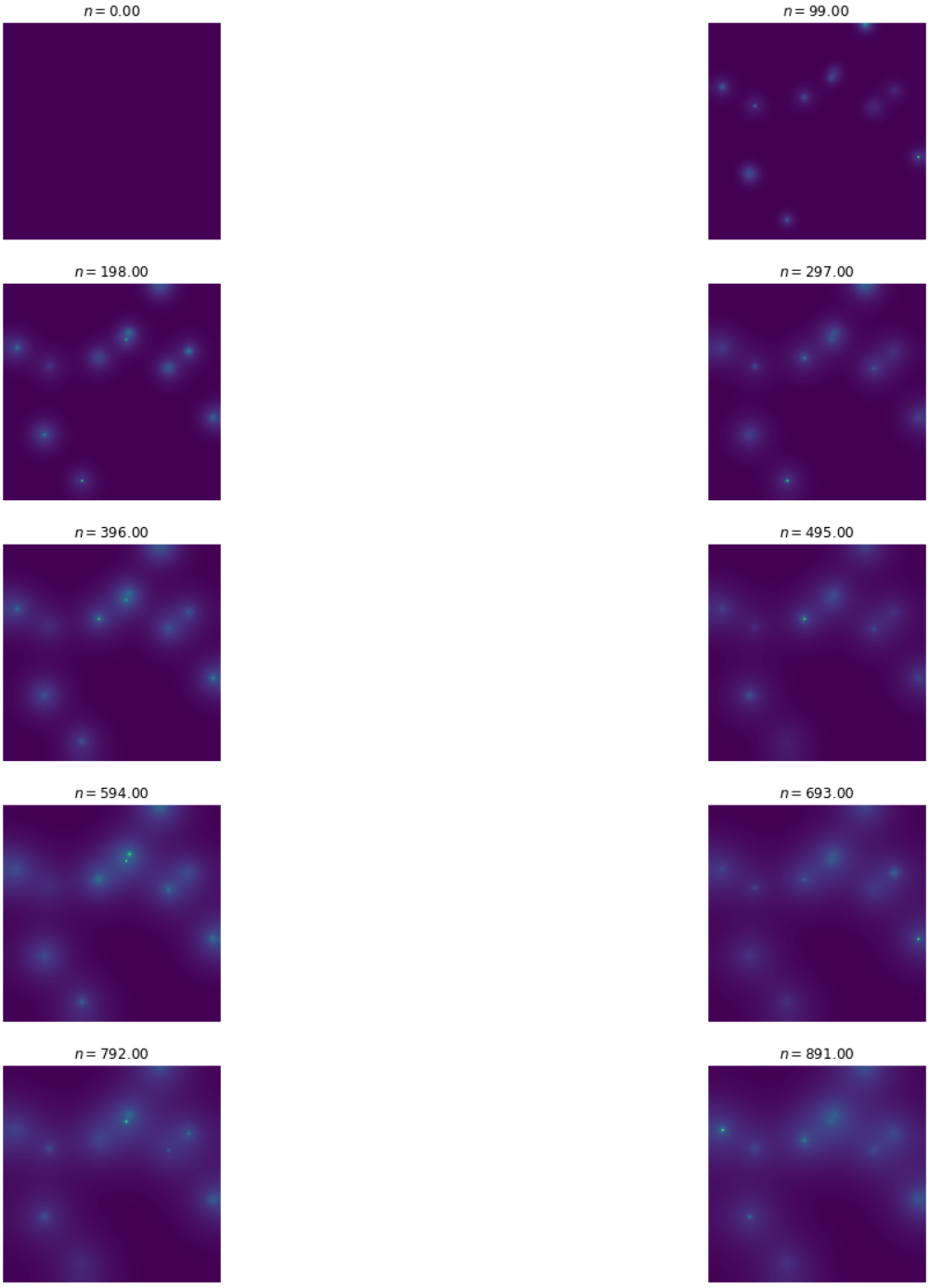

Figure 5.7: Change in Cancer Cell Distribution in Metastatic Site (Brain).

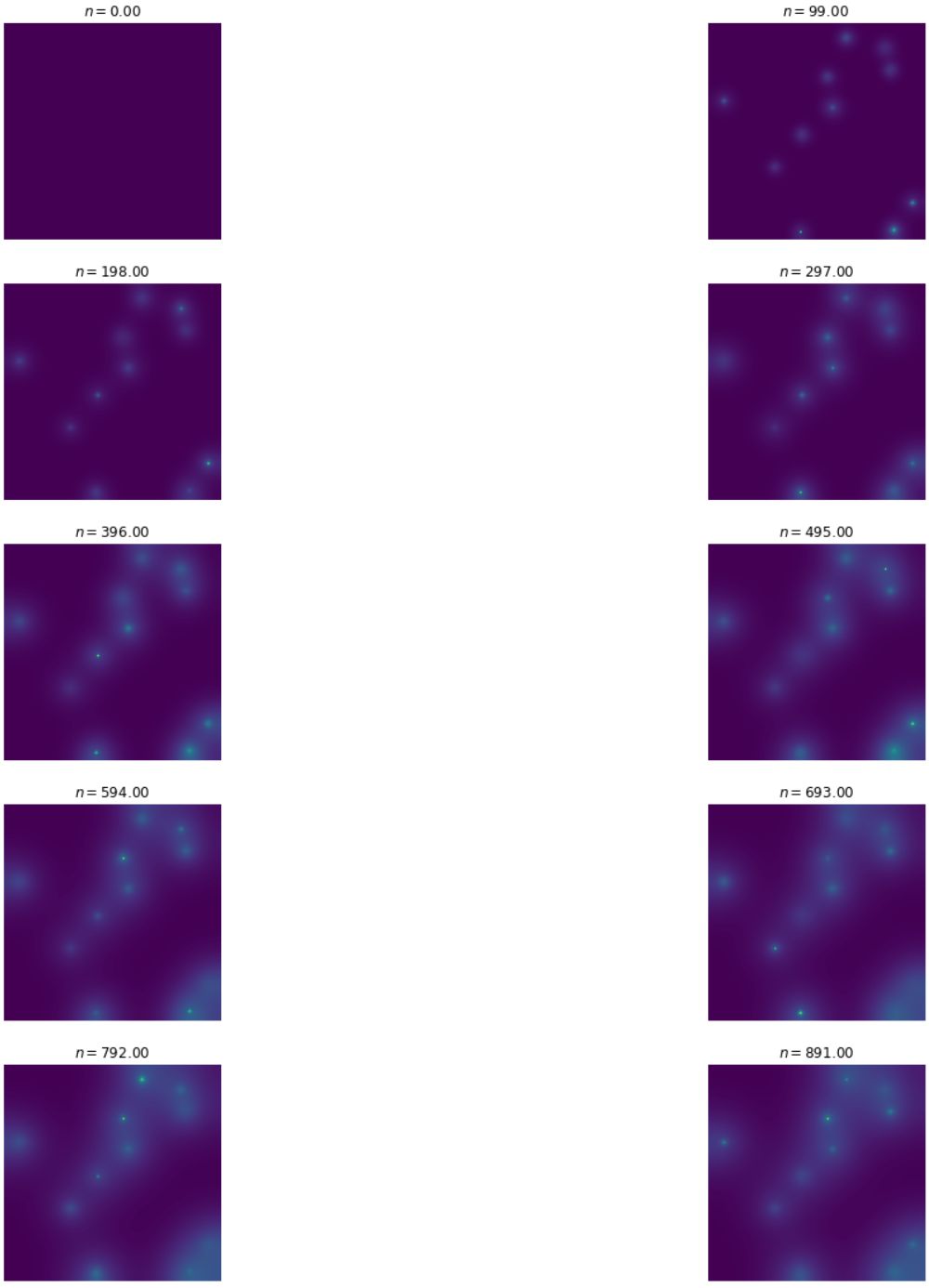

Figure 5.8: Change in Cancer Cell Distribution in Metastatic Site (Kidney).

Note that while each figure shows the presence of some micro-tumours, the scale is not the same for each organ. Therefore, despite having qualitatively similar behaviour, the exact number of cells differ.

While the model has clinically relevant results for the gut, the potential spread from cancers originating in other organs must be considered to determine the model's overall performance. We, therefore, analyse data sourced from the Human Cancer Metastasis Database (HCMDB) [93]. Our focus is solely on cancers arising in and metastasising to the organs under study. We use the data to determine the common metastasis sites for each organ and determine whether the model's predictions align with these findings.

When analysing the HCMDB data, we first filter the primary and secondary sites for only the organs under study. After that, for each primary site, we determine the percentage of secondary metastases formed at each secondary site. Regions such as the small intestine, stomach and colorectum are all classified as cancer of the gut to align with the cardiac anatomy model in [39]. The results are summarised in the proceeding table.

Primary Site	**Secondary Site**				
	Brain	Gut	Kidney	Liver	Lung
Brain	100%	0%	0%	0%	0%
Gut	0.16%	0.25%	0%	90.76%	8.83%
Kidney	0%	0%	0.99%	8.42%	90.59%
Liver	0%	0%	0%	8.89%	91.111%
Lung	100%	0%	0%	0%	0%

We now contrast the information from the preceding table with the outputs generated by the model. The results are expressed by counting the number of cells in each secondary location and expressing this as a percentage of the total number of cells. This information is summarised in Figure 5.9. For each primary site, we compare the findings from the simulation against the HCMDB data. Next, we contextualise these results with the relevant tumour pathology; this allows us to draw inferences on the model's performance and, where possible, make conclusions on the role of hematogenous metastasis for cancers originating in the selected primary sites.

The HCMDB analysis notes that cancers from the gut primarily metastasise

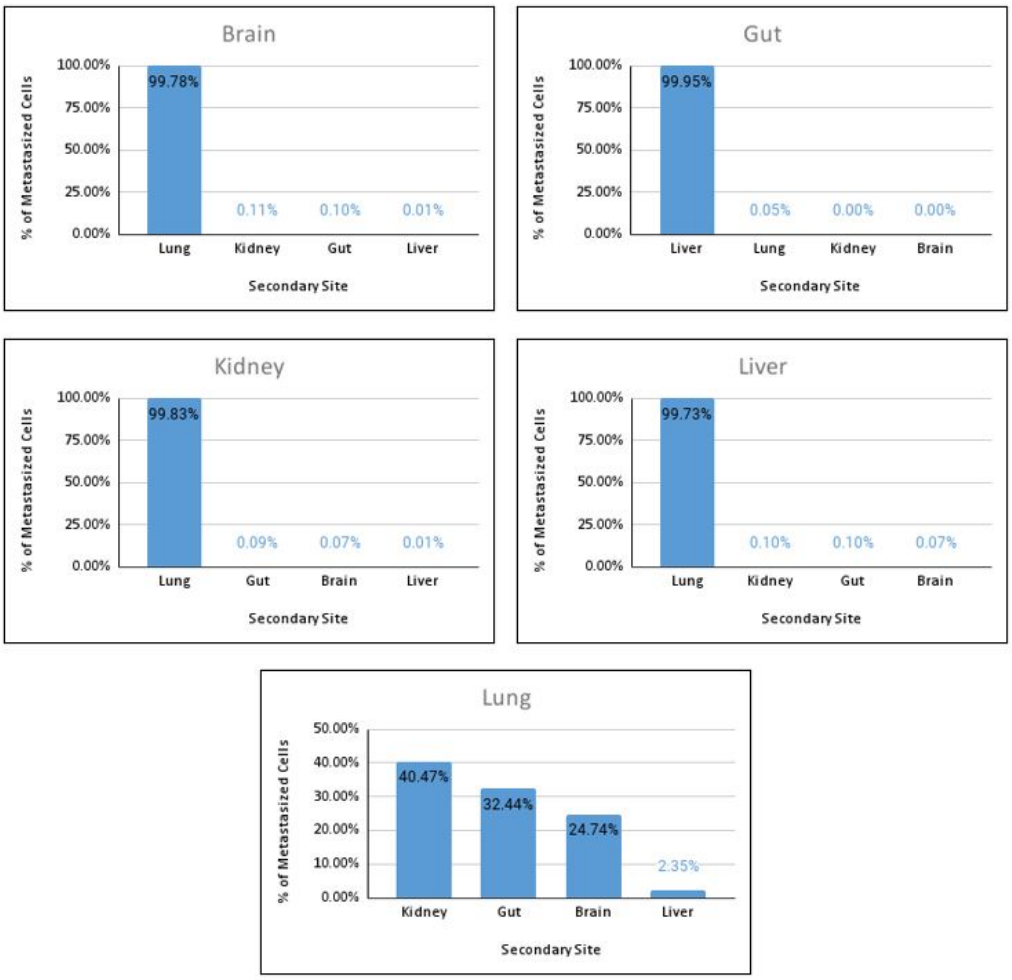

Figure 5.9: Percentage of cancer cells found in secondary sites for each of the organs under study.

to the liver. Tumours originating in the kidney and the liver tend to metastasise to the lung. In all records of interest, lung cancer spreads to the brain. Of particular interest is the brain, which displayed local metastasis for all of the observations in the data set. The simulation displays similar results for the gut, kidney and liver and conflicting views for the lung and brain. We discuss both the contradictory and complementary results.

When selecting the brain as the primary site, the simulation shows that most metastatic cells colonise the lung. This finding can be ascribed to the large volume of blood the lungs receive from venous circulation. However, the HCMDB data shows that the overwhelming majority of brain cancers

produce only local metastases. A review of the literature confirms that cancers of the brain, or central nervous system (CNS), rarely produce secondary metastases. This phenomenon is attributed to a host of reasons. Firstly, the brain lacks specific ECM components which facilitate the migration of cancer cells into the bloodstream; thus, while cancer can proliferate, it cannot easily invade [62]. Another explanation for the observed rarity of brain metastases is the low survival rate of brain cancer. Patients typically lead much shorter lifespans; thus, cancer does not have sufficient time to metastasise [51]. Both these factors are not considered in the model, as, aside from varying the type of diffusive behaviour at each organ, we do not consider organs for which diffusion is complex. The lifespan of patients is also excluded from our model parameters. We can thus conclude that the brain favours neither hematogenous nor lymphatic metastases as the primary method of spread.

As discussed earlier in the section, our model predicted the liver as the site that receives the largest concentration of metastatic cells from the gut. After the liver, the lung receives the most significant proportion of tumour cells. These findings align with the HCMDB data, as the liver is the most common metastatic site for colorectal cancers, while the lung is the second most prevalent site. While our model does imply the possibility of metastatic lung cancer, it does not occur independently of liver metastases. In reality, isolated lung metastases are relatively rare [77]. In our analysis, they represent 8.83% of all metastatic colon cancers. One possibility for this discrepancy lies in our grouping of cancers originating in the gut. Cancers of the rectum, as opposed to the colon, are more likely to result in lung metastasis [77]. This observation can be attributed to the 'seed and soil' hypothesis, which we reviewed in Chapter 1. The hypothesis states that the micro-environment of the secondary site must be hospitable to the tumour cells from the primary site. We can therefore infer that the lung is likely a favourable soil for the cancer cells originating in the rectum. The colonisation of the lungs may also arise from lymphatic metastasis. Cancer cells from the lymph nodes enter venous circulation via the subclavian vein; consequently, the first capillaries the cells come into contact with is in the lung [55]. From our analysis, we may conclude that hematogenous metastasis is likely the cause of secondary metastasis to the liver. It is unlikely that hematogenous metastasis is solely responsible for isolated metastases to the lungs, as other metastatic mechanisms are probably at play.

Primary lung cancers generally metastasise to the brain, bone, and adrenal glands [65]. Since the bone and adrenal glands are beyond the scope of

this study, we removed them from the data set and the simulation. Our simulation identified many cancer cells in all organs except the liver; this is in line with the estimated cardiac output to these organs displayed in Figure 4.1. The Kidneys received the most blood, at 22%, with the gut following closely behind at 21%. The brain receives 14% and the liver 6%. Lung cancer-specific data, however, shows that the most common metastatic sites for the lung are the CNS and the liver, with 47% and 35% prevalence in the data [69]. Although this has been shown to differ based on the histology of the cancer [53]. The liver micro-environment may be hospitable to lung cancer. Alternatively, the spread may be driven by the lymph nodes. Of particular importance, however, is metastasis to the brain. The brain is the most common secondary site for lung cancer. The mechanisms which drive this particular spread are not fully understood. One proposition for the high incidence of secondary brain tumours is the seed and soil hypothesis. The brain is likely a favourable soil for lung cancer [19]. Unfortunately, the model does not capture the complexities of the seed and soil hypothesis and the nuances of differing micro environments; this shows that these factors play a crucial role in the metastatic cascade, as it supersedes the results we anticipate from a purely hematogenous spread.

Cancers of the liver metastasise mainly to the lung. With the brain being the least likely secondary location [91]. These findings show some alignment to the model, as the lung receives the highest proportion of cells while the brain receives the lowest. This finding shows good alignment with clinical data and implies that hematogenous spread is a strong driver for liver metastases. Based on our model, The kidney and gut receive the second and third highest proportion; this, however, is not aligned with the HCMDB, as no metastases to these sites were identified. It is worth noting that the model predicted very small proportions in these organs.

For the kidney, our model produced the most number of metastases in the lung, followed by the gut, brain and liver. In the HCMDB data, the kidney metastasizes most frequently to the lung and liver. The brain is also a common secondary site for cancer of the kidney [74], despite being absent from the HCMDB data we analysed. Venous blood from the colic vein drains directly into the hepato-portal vein; this potentially explains why isolated liver metastases are common for kidney cancer patients. These veins were excluded from the simulation, and hence this behaviour is not reflected. Since this is still a vascular pathway, We can conclude that hematogenous spread predicted by the simulation could play a vital role in both liver and kidney metastasis. It is important to note that lymphatic spread may also

be a driving factor for lung metastases.

5.2 Varying Blood Velocity

In this section, we review the effects of blood velocity on the process of metastasis. The velocity of blood in each vessel is varied across biologically realistic ranges. We run the simulation using the lower and upper bounds for velocity. For consistency, we initialise cancer in the gut. These values are compared against the cancer cell concentration when using the average blood velocity, allowing us to determine the net effect of varying the velocity. The proceeding table contains the lower, average, and upper values of blood velocity in the relevant veins and arteries. Where values could not be sourced for velocity, we selected values within a reasonable range for blood velocity, as per some of the velocities identified in [27], while adhering to the CFL condition. The qualitative dynamics of the system were not appreciably affected by the choice of these values, although no formal sensitivity analysis was conducted.

Vessel Name	**Lower Bound (cm/s)**	**Average (cm/s)**	**Upper Bound (cm/s)**	**Reference**
Pulmonary Artery	10	33.5	57	[27]
Pulmonary Vein	10	15	20	N/A
Renal Artery	40	50	60	[1]
Renal Vein	10	15	20	N/A
Carotid Artery	80	100	120	[9]
Jugular	10	15	20	N/A
Abdominal Aorta	24	28	32	[75]
Hepato-portal Vein	20	30	40	[40]
Renal Vein	10	15	20	N/A

Running the simulation using the lower, average and upper velocities produced the results in Figure 5.10. We express these values as the percentage difference between low and high-velocity outputs and the average velocity output. This comparison gives us a clear indication of the impact of velocity in the simulation.

From these observations, we note that cancer did not metastasise to the lungs, kidney, and brain for higher velocity ranges, as there was a 100% decrease in cell concentration on those organs. There was, however, a very significant increase in cell concentration in the liver. At lower velocities, there was a substantial increase in the cell concentration at all locations. The cell concentration on the gut remained relatively consistent across each scenario.

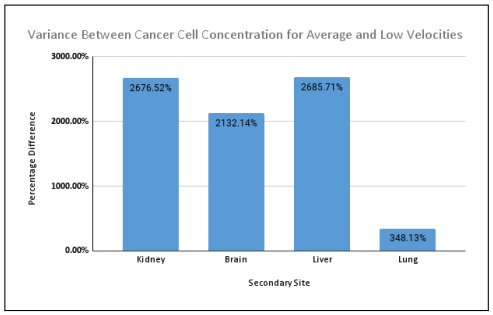

(a) Average vs Low Velocity

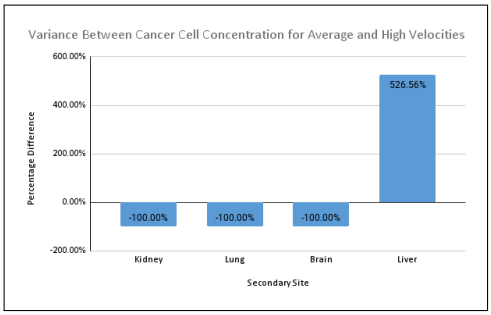

(b) Average vs High Velocity

Figure 5.10: Difference in Cell Concentration for Lower and Higher Velocities

In most cases, the model predicted an inverse relationship between blood velocity and cancer cell concentration, except for the liver at a high blood velocity. This discrepancy is possibly due to the proximity of the liver to the gut. The relationship between blood velocity and cancer spread is not well defined, and thus corroborative evidence is challenging to procure. These findings indicate that sustained variations in blood velocity can impact the spread of cancer. Since the simulation predicts that using higher velocities significantly lowers the metastatic potential of cancer, we can assume that this may have some bearing on metastatic inefficiency.

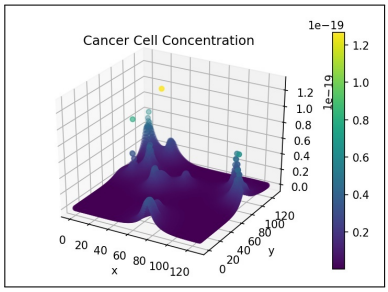

(a) Brain

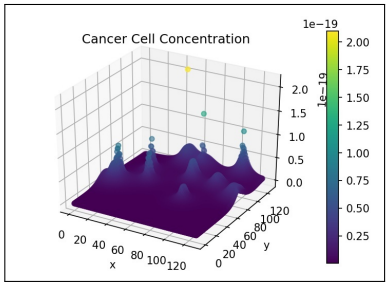

(b) Kidney

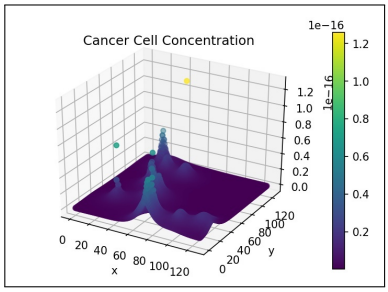

(c) Lung

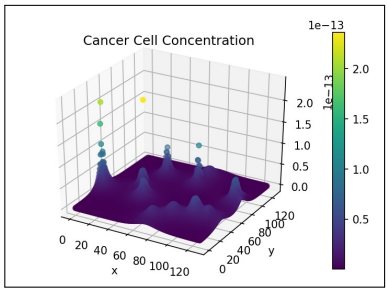

(d) Liver

Figure 5.11: Cell Concentration for Normal Velocities

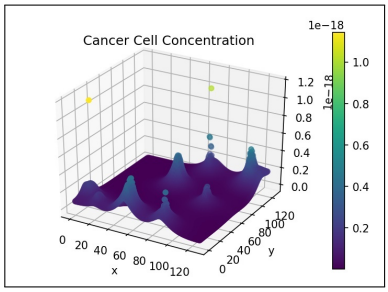

(a) Brain

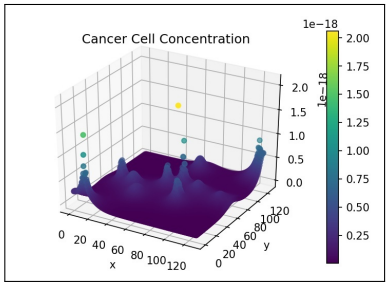

(b) Kidney

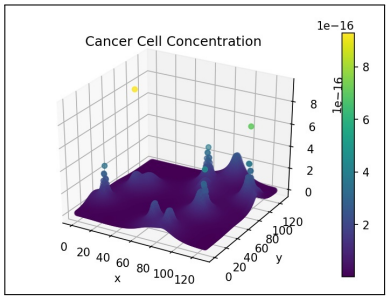

(c) Lung

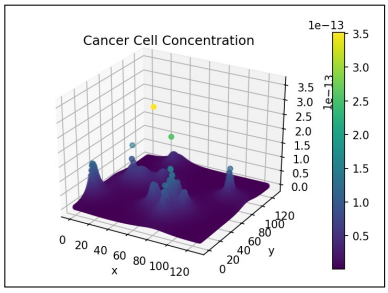

(d) Liver

Figure 5.12: Cell Concentration for Lower Velocities

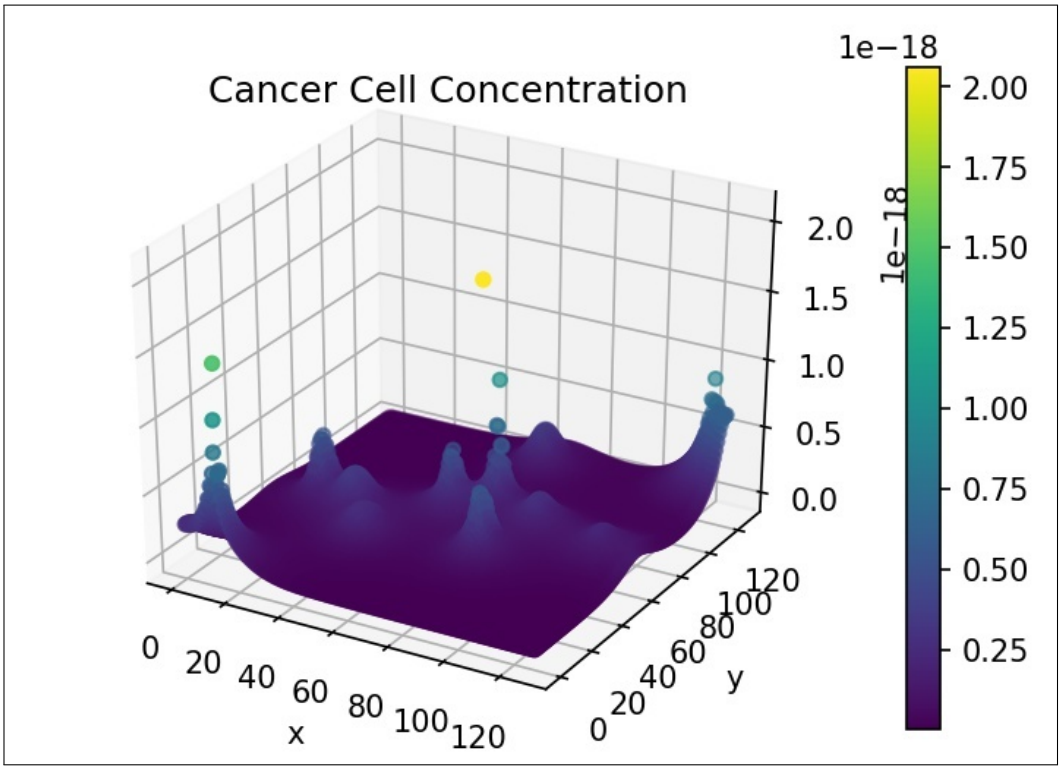

Figure 5.13: Cell Concentration in Liver at Higher Velocities

Figures 5.11 - 5.13 provide a 3-dimensional view of the micro-tumours that formed at each organ for the various blood velocities. This shows, qualitatively, the impact velocity can have.

5.3 Varying Diffusive Conditions

Thus far, we assumed that cancers exhibit isotropic diffusion. This assumption is not always valid, as some cancers diffuse anisotropically. For example, certain brain cancers - known as gliomas [70]. To study this effect on metastasis, we initialise cancer in a primary site and change the diffusion tensor to allow for anisotropic diffusion. The cancer cell concentration is aggregated and contrasted against the isotropic case. Similar to the previous sections, we initialise cancer in the gut. To achieve anisotropic diffusion, we set the value of a in the diffusion tensor to 0.1. This increases diffusion 10-fold in the y-direction [64].

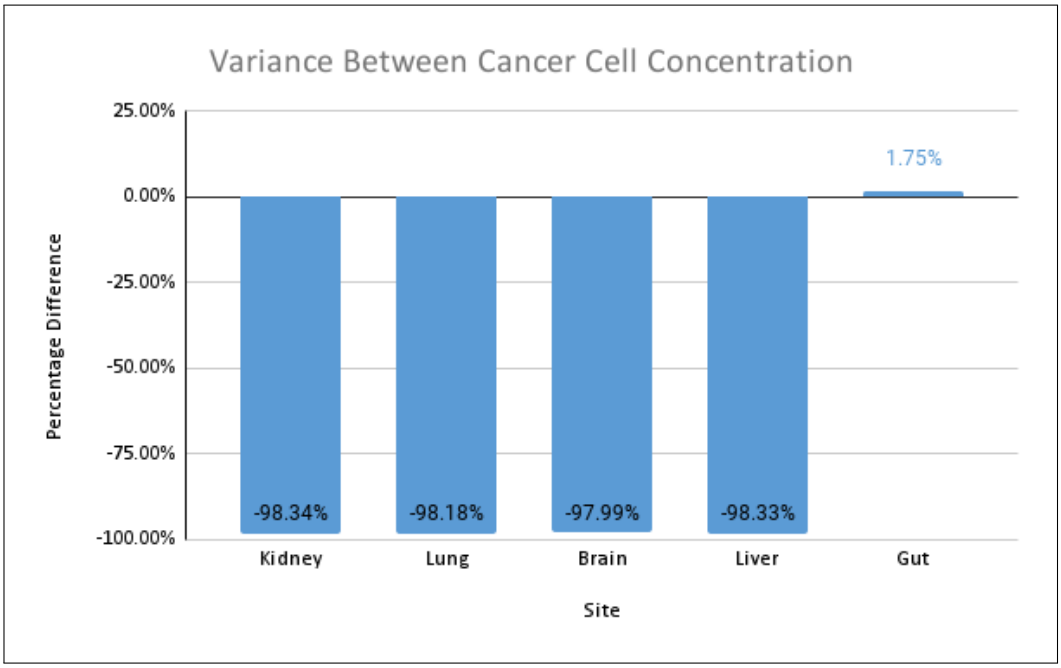

Figure 5.14: Percentage Difference between Cancer Cell Concentration in all Locations for Anisotropic and Isotropic Diffusion

Figure 5.14 displays the difference in cell concentration for both types of diffusion. There is a consistent decrease of around 98% of cancer cells in secondary locations for anisotropic diffusion. The primary site displays a slight increase in cell concentration. Figures 5.15 and 5.16 provide a general diffusion pattern for anisotropic diffusion on a primary and secondary site. We focus on the gut and liver, as the liver's behaviour indicates the general diffusive behaviour we observed in all the secondary sites.

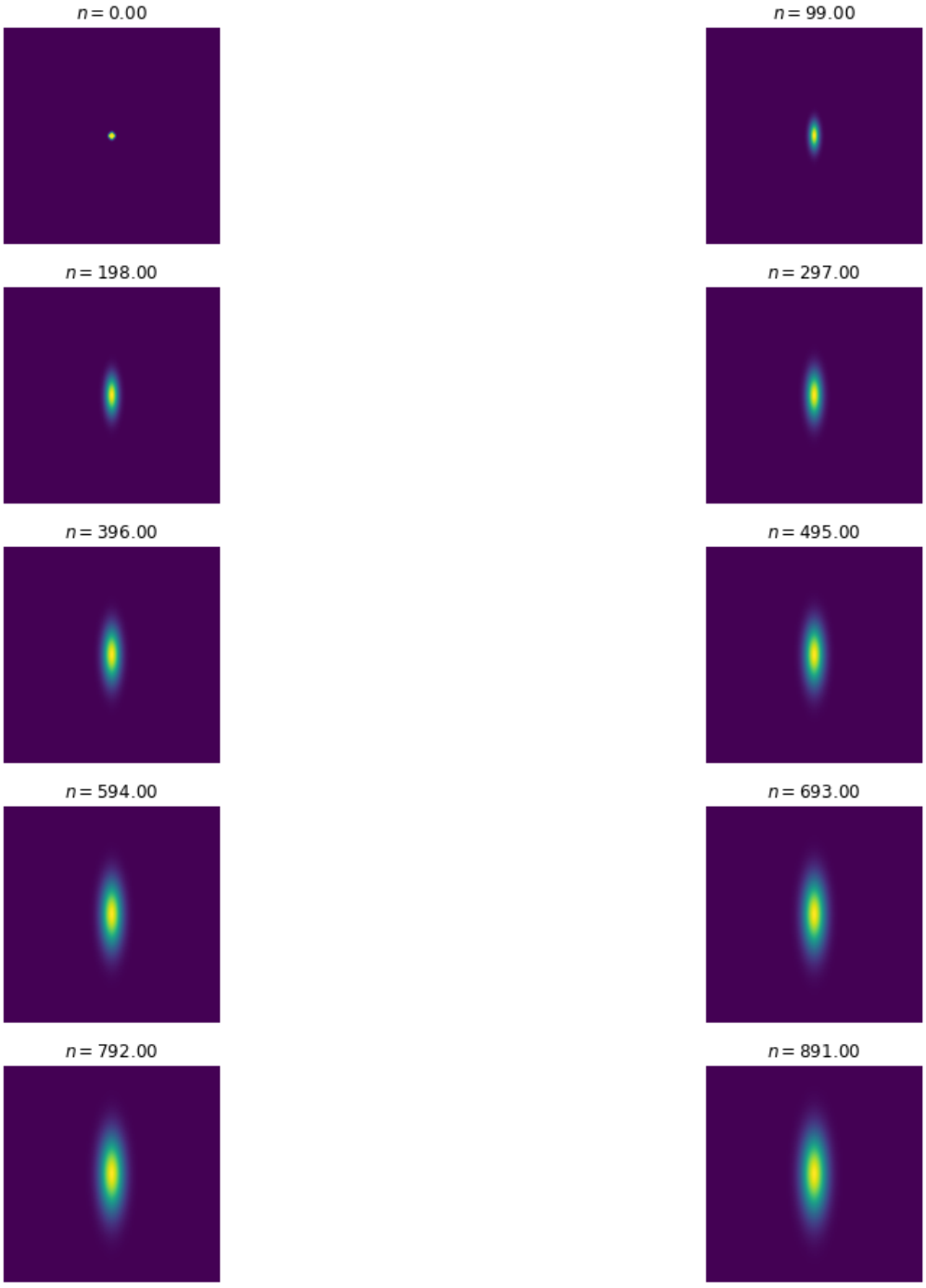

Figure 5.15: Change in Cancer Cell Distribution in Primary Site (Gut).

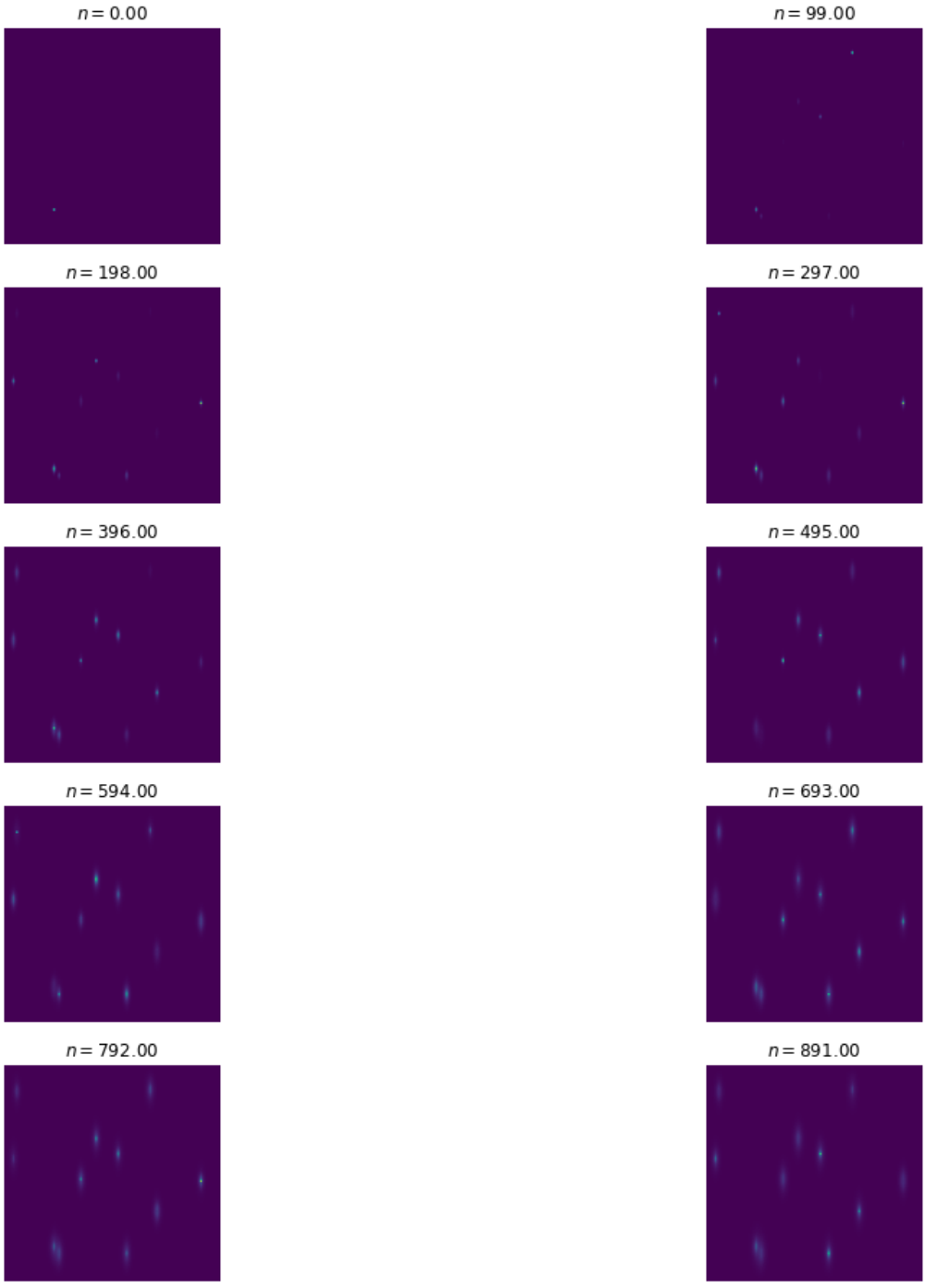

Figure 5.16: Change in Cancer Cell Distribution in Metastatic Site (Liver).

In Figure 5.15 the reinforced diffusion in the y-direction is clear. To understand why there is a decrease in cell concentration, we determine the number of intravasated cells and the number of blood vessels that have been reached for both cases. We focus on these as the diffusive behaviour directly impacts the number of cancer cells that arrive at the vessels and the number of times the vessels are reached. The general behaviour is shown in Figure 5.17.

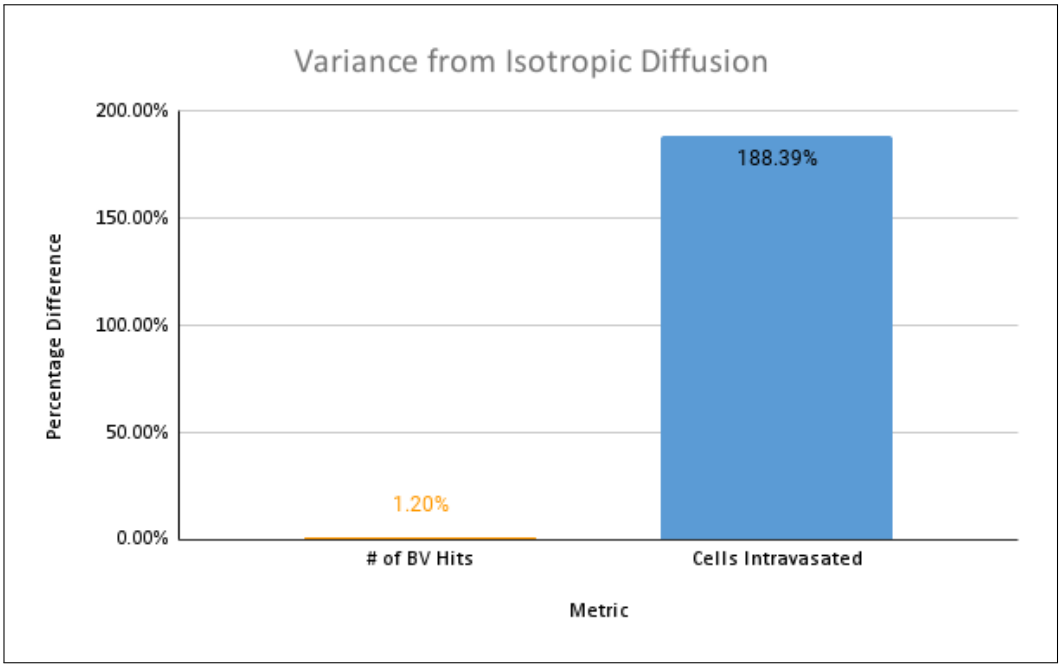

Figure 5.17: Percentage Difference between the Number of Blood Vessel Hits and Cells Intravasated for Anisotropic vs Isotropic Diffusion

We note there is a slight increase in the number of times a blood vessel is reached and a significant increase in the number of intravasated cells. This behaviour is likely due to the increased diffusion in the y-direction. The cancer cells can reach blood vessels located at the upper and lower quadrants of the region. Since cancer still diffuses in the x-direction, some intravasation occurs at blood vessels in these regions. The slight increase in blood vessel hits and the large concentration of cells that reach the blood vessels in the upper and lower quadrants are potentially responsible for the considerable increase in extravasated cells. Since we note an increase in both these metrics, we can conclude that these factors do not decrease cell concentration in the secondary sites.

These findings deduce that anisotropic diffusion may result in a slightly

higher concentration of cancer cells in the primary site but a lower concentration of cells in the secondary site. This type of diffusion also causes a larger proportion of cells to undergo intravasation. Anisotropic tumours can thus be considered less efficient for metastasis. Secondary sites appear to be a hostile environment for tumours that diffuse anisotropically; this is consistent with behaviour we note for gliomas, as they do not generally produce secondary metastases. Diffusive behaviour can be responsible for metastatic inefficiency, a factor that is not generally considered.

In this chapter, we have compared the results of our model against clinical data and used the model to study the impact of various factors on the large-scale spread of cancer. These factors include the velocity of blood and the diffusive behaviour of the cancer itself. We found a good correlation to clinical data for some organs and examined the factors that could impact the spread for other sites. We noted that there is, in general, an inverse relationship between blood velocity and cancer cell concentration in secondary locations. Finally we found that anisotropic tumours are poor seeds for the secondary sites under consideration, as it renders metastasis less efficient. In the following chapter, we conclude the research presented in this dissertation.

Chapter 6

Conclusion

This research aimed to develop a holistic model of metastasis, which characterises the spread of cancer from the primary site to secondary locations. The impetus for this model is to elucidate the process of metastasis. Mainly, we focused on the following research questions:

- What is the most likely sequence of secondary locations given some primary tumour location?
- How does the rate of blood flow impact the process of metastasis?
- What global effect does differing the diffusive behaviour of cancer cells have on the overall spread?

Regarding the first question, we find that the simulation aligns with previous models for cancer growth on the primary site. We also observed a substantial correlation with the secondary sites for cancer of the gut and liver against clinical data. There were some deviations for the brain, lung and kidney. These deviations are due to the unique environment of the brain, potentially the 'seed and soil' hypothesis for the lung and some vasculature we excluded for the kidney. Despite the excluded vasculature, we note that the model does show some good alignment with the clinical data. The model allows us to understand the impact of hematogenous metastasis for the various organs under study. From these results, we can infer that hematogenous metastasis is a primary driver for metastasis of the gut, liver and potentially the kidney. Metastasis is very unlikely for the brain, while other factors are more critical

for cancer spread from the lung. These factors include the above-mentioned 'seed and soil' hypothesis and potentially lymphatic spread.

We found an inverse relationship between blood velocity and cancer cell concentration concerning the second of our research questions. This case holds except for when cancer originates in the gut and spreads to the liver at high blood velocities. This behaviour is possibly due to the proximity of the gut and liver. Since there is a lack of clinical data, we cannot contrast the model against practical observations. We can conclude that it is likely that blood flow velocity does affect cancer spread. The blood velocity use case also demonstrates how this framework can simulate patient-specific information.

Our final research question holds clinical significance because some cancers display anisotropic diffusion. Here the model predicted an overall decrease in the cancer cell concentration at the secondary sites. This behaviour holds for some cancers that diffuse anisotropically, particularly gliomas of the brain. We have noticed a slight increase in cancer cells in the primary site and a sizable increase in intravasation from the primary site. This behaviour shows us the effect of varying diffusion on the overall spread. To our knowledge, the existing body of research on mathematical oncology has not explored the impact of anisotropic diffusion on metastasis.

The impact these changes have on the overall spread of cancer does affirm the difficulty in fully understanding the process, as we have noticed how small changes in some of these conditions, such as blood velocity, can lead to differing outcomes. The model does provide a good framework for exploring how some of these factors, which may be patient or case-specific, can be simulated for mechanistic purposes. Overall, this research allows practitioners to study the global effects of cancer in a manner that has hitherto been difficult to simulate. However, our focus on the global impact does restrict the histological factors we can consider at a smaller scale. These exclusions can harm accuracy, as we may inadvertently omit potentially important information.

Based on our research, we can draw conclusions that may aid medical practitioners and researchers in mathematical oncology. Medical practitioners should consider the diffusive nature of cancer when deciding the potential metastatic sequence cancer will follow as our analysis indicates that the spread to other sites for cancers that diffusive anisotropically is generally slower. For researchers of mathematical oncology, we have introduced a framework that encapsulates the global behaviour of cancer. This methodology can be expanded on to include other behaviour at the cellular level; for example, cancer cells often intravasate as clusters. These clusters can

impact the process of intravasation and the survival probability of cells in the vasculature [26].

Furthermore, other means of transportation, particularly transport through the lymph, can significantly advance the model's scope. We use a simple abstraction of blood dynamics in this model - further research can expand this to include more appropriate fluid dynamics. In addition to fluid dynamics, there are other biological factors cancer experiences in the bloodstream which we have ignored - for example, the immune response that the patient expresses. Perhaps most interesting is the opportunity to include more patient-specific information. For example, a patient's unique vessel permissivity can determine the likelihood of the cell to intravasate.

Bibliography

[1] Al-Katib, S., Shetty, M., Jafri, S. M. A., and Jafri, S. Z. H. Radiologic assessment of native renal vasculature: a multimodality review. *Radiographics 37*, 1 (2017), 136–156.

[2] Alsarraj, J., and Hunter, K. W. Bromodomain-containing protein 4: A dynamic regulator of breast cancer metastasis through modulation of the extracellular matrix. *Int. J. Breast Cancer 2012* (2012), 670632.

[3] Anderson, A. R., Chaplain, M. A., Newman, E. L., Steele, R. J., and Thompson, A. M. Mathematical modelling of tumour invasion and metastasis. *Computational and mathematical methods in medicine 2*, 2 (2000), 129–154.

[4] Asllani, M., Challenger, J. D., Pavone, F. S., Sacconi, L., and Fanelli, D. The theory of pattern formation on directed networks. *Nature communications 5*, 1 (2014), 1–9.

[5] Balmain, A. The critical roles of somatic mutations and environmental tumor-promoting agents in cancer risk. *Nature genetics 52*, 11 (2020), 1139–1143.

[6] Baratchart, E., Benzekry, S., Bikfalvi, A., Colin, T., Cooley, L. S., Pineau, R., Ribot, E. J., Saut, O., and Souleyreau, W. Computational modelling of metastasis development in renal cell carcinoma. *PLoS computational biology 11*, 11 (2015), e1004626.

[7] Bartoszyński, R. On metastatic progression of cancer. *Advances in Applied Probability 17*, 2 (1985), 245–246.

[8] Bondy, J., and Murty, U. *Graph Theory with Applications.* The Macmillan Press Ltd., 1976.

[9] Brant, W. E. *The core curriculum, ultrasound.* Lippincott Williams & Wilkins, 2001.

[10] Britton, N. F. *Reaction-diffusion equations and their applications to biology.* Elsevier Academic Press Inc, 1986.

[11] Byrne, H. M. Biological inferences from a mathematical model for malignant invasion. *Invasion Metastasis 16* (1996), 209–22l.

[12] Chen, L., Blumm, N., Christakis, N., Barabasi, A., and Deisboeck, T. S. Cancer metastasis networks and the prediction of progression patterns. *British journal of cancer 101*, 5 (2009), 749–758.

[13] Choudhry, F. A., Grantham, J. T., Rai, A. T., and Hogg, J. P. Vascular geometry of the extracranial carotid arteries: an analysis of length, diameter, and tortuosity. *Journal of neurointerventional surgery 8*, 5 (2016), 536–540.

[14] Coccolini, F., Gheza, F., Lotti, M., Virzì, S., Iusco, D., Ghermandi, C., Melotti, R., Baiocchi, G., Giulini, S. M., Ansaloni, L., et al. Peritoneal carcinomatosis. *World journal of gastroenterology: WJG 19*, 41 (2013), 6979.

[15] Cooper, G. M., Hausman, R. E., and Hausman, R. E. *The cell: a molecular approach*, vol. 4. ASM press Washington, DC, USA:, 2007.

[16] Cope, C., and Isard, H. J. Left renal vein entrapment: a new diagnostic finding in retroperitoneal disease. *Radiology 92*, 4 (1969), 867–872.

[17] Croce, C. M. Oncogenes and cancer. *New England journal of medicine 358*, 5 (2008), 502–511.

[18] Easley, D., and Kleinberg, J. *Networks, crowds, and markets: Reasoning about a highly connected world*. Cambridge university press, 2010.

[19] Ebben, J. D., and You, M. Brain metastasis in lung cancer: building a molecular and systems-level understanding to improve outcomes. *The international journal of biochemistry & cell biology 78* (2016), 288–296.

[20] Enderling, H., and AJ Chaplain, M. Mathematical modeling of tumor growth and treatment. *Current pharmaceutical design 20*, 30 (2014), 4934–4940.

[21] Enderling, H., Anderson, A. R., Chaplain, M. A., Munro, A. J., and Vaidya, J. S. Mathematical modelling of radiotherapy

strategies for early breast cancer. *Journal of Theoretical Biology 241*, 1 (2006), 158–171.

[22] Ferlay, J., Colombet, M., Soerjomataram, I., Parkin, D. M., Piñeros, M., Znaor, A., and Bray, F. Cancer statistics for the year 2020: An overview. *International Journal of Cancer 149*, 4 (2021), 778–789.

[23] Fidler, I. J. The pathogenesis of cancer metastasis: the'seed and soil'hypothesis revisited. *Nature reviews cancer 3*, 6 (2003), 453–458.

[24] Fidler, I. J., and Poste, G. The "seed and soil" hypothesis revisited. *The lancet oncology 9*, 8 (2008), 808.

[25] Font-Clos, F., Zapperi, S., and La Porta, C. A. Blood flow contributions to cancer metastasis. *Iscience 23*, 5 (2020), 101073.

[26] Franssen, L. C., Lorenzi, T., Burgess, A. E., and Chaplain, M. A. A mathematical framework for modelling the metastatic spread of cancer. *Bulletin of mathematical biology 81*, 6 (2019), 1965–2010.

[27] Gabe, I. T., GAULT, J. H., ROSS JR, J., MASON, D. T., MILLS, C. J., SCHILLINGFORD, J. P., and BRAUNWALD, E. Measurement of instantaneous blood flow velocity and pressure in conscious man with a catheter-tip velocity probe. *Circulation 40*, 5 (1969), 603–614.

[28] Gameraddin, M. Normal abdominal aorta diameter on abdominal sonography in healthy asymptomatic adults: impact of age and gender. *Journal of Radiation Research and Applied Sciences 12*, 1 (2019), 186–191.

[29] Gatenby, R. A., and Gawlinski, E. T. A reaction-diffusion model of cancer invasion. *Cancer research 56*, 24 (1996), 5745–5753.

[30] Gerlee, P. The model muddle: in search of tumor growth laws. *Cancer research 73*, 8 (2013), 2407–2411.

[31] Gompertz, B. Xxiv. on the nature of the function expressive of the law of human mortality, and on a new mode of determining the value of life contingencies. in a letter to francis baily, esq. frs &c. *Philosophical transactions of the Royal Society of London*, 115 (1825), 513–583.

[32] Griffiths, A., Miller, J., Suzuki, D., Lewontin, R., and Gelbart, W. *Mendel's experiments*. WH Freeman, 2000.

[33] Hanahan, D., and Weinberg, R. A. The hallmarks of cancer. *cell 100*, 1 (2000), 57–70.

[34] Harouaka, R. A., Nisic, M., and Zheng, S.-Y. Circulating tumor cell enrichment based on physical properties. *Journal of laboratory automation 18*, 6 (2013), 455–468.

[35] Hart, D., Shochat, E., and Agur, Z. The growth law of primary breast cancer as inferred from mammography screening trials data. *British journal of cancer 78*, 3 (1998), 382–387.

[36] Heaton, L. L., López, E., Maini, P. K., Fricker, M. D., and Jones, N. S. Advection, diffusion, and delivery over a network. *Physical Review E 86*, 2 (2012), 021905.

[37] Hirsch, C. *Numerical computation of internal and external flows: The fundamentals of computational fluid dynamics*. Elsevier, 2007.

[38] Holly, J. M., Zeng, L., and Perks, C. M. Epithelial cancers in the post-genomic era: should we reconsider our lifestyle? *Cancer and Metastasis Reviews 32*, 3 (2013), 673–705.

[39] Iaizzo, P. A. *Handbook of cardiac anatomy, physiology, and devices*. Springer Science & Business Media, 2010.

[40] Iranpour, P., Lall, C., Houshyar, R., Helmy, M., Yang, A., Choi, J.-I., Ward, G., and Goodwin, S. C. Altered doppler flow patterns in cirrhosis patients: an overview. *Ultrasonography 35*, 1 (2016), 3.

[41] Iwata, K., Kawasaki, K., and Shigesada, N. A dynamical model for the growth and size distribution of multiple metastatic tumors. *Journal of theoretical biology 203*, 2 (2000), 177–186.

[42] Karaman, S., Detmar, M., et al. Mechanisms of lymphatic metastasis. *The Journal of clinical investigation 124*, 3 (2014), 922–928.

[43] Kim, Y., Williams, K. C., Gavin, C. T., Jardine, E., Chambers, A. F., and Leong, H. S. Quantification of cancer cell extravasation in vivo. *Nature protocols 11*, 5 (2016), 937–948.

[44] Kondo, S., and Miura, T. Reaction-diffusion model as a framework for understanding biological pattern formation. *science 329*, 5999 (2010), 1616–1620.

[45] Kroese, D. P., Brereton, T., Taimre, T., and Botev, Z. I. Why the monte carlo method is so important today. *Wiley Interdisciplinary Reviews: Computational Statistics 6*, 6 (2014), 386–392.

[46] Kuang, Y., Nagy, J. D., and Eikenberry, S. E. *Introduction to mathematical oncology*. Chapman and Hall/CRC, 2018.

[47] Liotta, L. A., Saidel, G. M., and Kleinerman, J. Stochastic model of metastases formation. *Biometrics* (1976), 535–550.

[48] Liu, X.and Fu, A., How, Y., and Luo, K. Effects of hemodynamic shear stress on circulating tumor cells.

[49] Lopez-Camarillo, C., and Arechaga-Ocampo, E. *Oncogenomics and Cancer Proteomics: Novel Approaches in Biomarkers Discovery and Therapeutic Targets in Cancer*. BoD–Books on Demand, 2013.

[50] Malek, A. *Experimental metastasis: modeling and analysis*. Springer, 2013.

[51] Mentrikoski, M., Johnson, M. D., Korones, D. N., and Scott, G. A. Glioblastoma multiforme in skin: a report of 2 cases and review of the literature. *The American Journal of Dermatopathology 30*, 4 (2008), 381–384.

[52] Mikuła-Pietrasik, J., Uruski, P., Tykarski, A., and Książek, K. The peritoneal "soil" for a cancerous "seed": a comprehensive review of the pathogenesis of intraperitoneal cancer metastases. *Cellular and Molecular Life Sciences 75*, 3 (2018), 509–525.

[53] Milovanovic, I. S., Stjepanovic, M., and Mitrovic, D. Distribution patterns of the metastases of the lung carcinoma in relation to histological type of the primary tumor: An autopsy study. *Annals of thoracic medicine 12*, 3 (2017), 191.

[54] Müller, L. O., and Toro, E. F. A global multiscale mathematical model for the human circulation with emphasis on the venous system. *International journal for numerical methods in biomedical engineering 30*, 7 (2014), 681–725.

[55] Naxerova, K., Reiter, J. G., Brachtel, E., Lennerz, J. K., Van De Wetering, M., Rowan, A., Cai, T., Clevers, H., Swanton, C., Nowak, M. A., et al. Origins of lymphatic and distant metastases in human colorectal cancer. *Science 357*, 6346 (2017), 55–60.

[56] Newton, P. K., Mason, J., Bethel, K., Bazhenova, L., Nieva, J., Norton, L., and Kuhn, P. Spreaders and sponges define metastasis in lung cancer: a markov chain monte carlo mathematical model. *Cancer research 73*, 9 (2013), 2760–2769.

[57] Newton, P. K., Mason, J., Bethel, K., Bazhenova, L. A., Nieva, J., and Kuhn, P. A stochastic markov chain model to describe lung cancer growth and metastasis. *PloS one 7*, 4 (2012), e34637.

[58] Nishida, N., Yano, H., Nishida, T., Kamura, T., and Kojiro, M. Angiogenesis in cancer. *Vascular health and risk management 2*, 3 (2006), 213.

[59] Orr, F. W., Buchanan, M. R., and Weiss, L. *Microcirculation in cancer metastasis*. CRC press, 1991.

[60] Paget, S. The distribution of secondary growths in cancer of the breast. *The Lancet 133*, 3421 (1889), 571–573.

[61] Painter, K., and Hillen, T. Mathematical modelling of glioma growth: the use of diffusion tensor imaging (dti) data to predict the anisotropic pathways of cancer invasion. *Journal of theoretical biology 323* (2013), 25–39.

[62] Pansera, F., and Pansera, E. An explanation for the rarity of extraaxial metastases in brain tumors. *Medical hypotheses 39*, 1 (1992), 88–89.

[63] Patankar, S. V. *Numerical heat transfer and fluid flow*. CRC press, 2018.

[64] Pera, D., Málaga, C., Simeoni, C., and Plaza, R. G. On the efficient numerical simulation of heterogeneous anisotropic diffusion models for tumor invasion using gpus. *Rendiconti di Matematica e delle sue Applicazioni 40*, 3-4 (2019), 233–255.

[65] Popper, H. H. Progression and metastasis of lung cancer. *Cancer and Metastasis Reviews 35*, 1 (2016), 75–91.

[66] Quaranta, V., Weaver, A. M., Cummings, P. T., and Anderson, A. R. Mathematical modeling of cancer: the future of prognosis and treatment. *Clinica Chimica Acta 357*, 2 (2005), 173–179.

[67] Raj, A., Kuceyeski, A., and Weiner, M. A network diffusion model of disease progression in dementia. *Neuron 73*, 6 (2012), 1204–1215.

[68] Rejniak, K. A., and Anderson, A. R. Hybrid models of tumor growth. *Wiley Interdisciplinary Reviews: Systems Biology and Medicine 3*, 1 (2011), 115–125.

[69] Riihimäki, M., Hemminki, A., Fallah, M., Thomsen, H., Sundquist, K., Sundquist, J., and Hemminki, K. Metastatic sites and survival in lung cancer. *Lung cancer 86*, 1 (2014), 78–84.

[70] Roniotis, A., Manikis, G. C., Sakkalis, V., Zervakis, M. E., Karatzanis, I., and Marias, K. High-grade glioma diffusive modeling using statistical tissue information and diffusion tensors extracted from atlases. *IEEE Transactions on Information Technology in Biomedicine 16*, 2 (2011), 255–263.

[71] Saidel, G. M., Liotta, L. A., and Kleinerman, J. System dynamics of a metastatic process from an implanted tumor. *Journal of theoretical biology 56*, 2 (1976), 417–434.

[72] Schwab, M., Ed. *Gompertzian Growth Curve*. Springer Berlin Heidelberg, 2011.

[73] Simonsen, I. Diffusion and networks: A powerful combination! *Physica A 357*, 2 (2005), 317–330.

[74] Sivaramakrishna, B., Gupta, N. P., Wadhwa, P., Hemal, A. K., Dogra, P. N., Seth, A., Aron, M., Kumar, R., et al. Pattern of metastases in renal cell carcinoma: a single institution study. *Indian journal of cancer 42*, 4 (2005), 173.

[75] Stein, P. D., Sabbah, H. N., Anbe, D. T., and Walburn, F. J. Blood velocity in the abdominal aorta and common iliac artery of man. *Biorheology 16*, 3 (1979), 249–255.

[76] Szabo, F. *The linear algebra survival guide: illustrated with Mathematica*. Academic Press, 2015.

[77] Tan, K. K., Lopes Jr, G. d. L., and Sim, R. How uncommon are isolated lung metastases in colorectal cancer? a review from database of 754 patients over 4 years. *Journal of gastrointestinal surgery 13*, 4 (2009), 642–648.

[78] Tucker, W. D., Weber, C., and Burns, B. Anatomy, thorax, heart pulmonary arteries. *StatPearls [Internet]* (2020).

[79] Turing, A. M. The chemical basis of morphogenesis. *Bulletin of mathematical biology 52*, 1 (1990), 153–197.

[80] Valastyan, S., and Weinberg, R. A. Tumor metastasis: molecular insights and evolving paradigms. *Cell 147*, 2 (2011), 275–292.

[81] Valderrama-Treviño, A. I., Barrera-Mera, B., Ceballos-Villalva, J. C., and Montalvo-Javé, E. E. Hepatic metastasis from colorectal cancer. *Euroasian journal of hepato-gastroenterology 7*, 2 (2017), 166.

[82] Vogelstein, B., and Kinzler, K. W. The multistep nature of cancer. *Trends in genetics 9*, 4 (1993), 138–141.

[83] Von Bertalanffy, L. Quantitative laws in metabolism and growth. *The quarterly review of biology 32*, 3 (1957), 217–231.

[84] Wan, X., Wang, W., Liu, J., and Tong, T. Estimating the sample mean and standard deviation from the sample size, median, range and/or interquartile range. *BMC medical research methodology 14*, 1 (2014), 1–13.

[85] Weigelt, B., Peterse, J. L., and Van't Veer, L. J. Breast cancer metastasis: markers and models. *Nature reviews cancer 5*, 8 (2005), 591–602.

[86] Weinberg, R. A. Tumor suppressor genes. *Science 254*, 5035 (1991), 1138–1146.

[87] Weinberg, R. A. *The biology of cancer*. WW Norton & Company, 2006.

[88] Wertheim, K. Y., and Roose, T. Can vegfc form turing patterns in the zebrafish embryo? *Bulletin of mathematical biology 81*, 4 (2019), 1201–1237.

[89] Wiig, H., and Swartz, M. A. Interstitial fluid and lymph formation and transport: physiological regulation and roles in inflammation and cancer. *Physiological reviews 92*, 3 (2012), 1005–1060.

[90] Wittekind, C., and Neid, M. Cancer invasion and metastasis. *Oncology 69*, Suppl. 1 (2005), 14–16.

[91] Wu, W., He, X., Andayani, D., Yang, L., Ye, J., Li, Y., Chen, Y., and Li, L. Pattern of distant extrahepatic metastases in primary liver cancer: a seer based study. *Journal of Cancer 8*, 12 (2017), 2312.

[92] Yang, J., and Counts, S. Predicting the speed, scale, and range of information diffusion in twitter. In *fourth international AAAI conference on weblogs and social media* (2010).

[93] Zheng, G., Ma, Y., Zou, Y., Yin, A., Li, W., and Dong, D. Hcmdb: the human cancer metastasis database. *Nucleic acids research 46*, D1 (2018), D950–D955.